Solving parametric problems in building renovation with a spectral reduced-order method

Suelen Gasparin, Julien Berger, Rafik Belarbi, Denys Dutykh, Nathan Mendes

Solving parametric problems in building renovation with a spectral reduced-order method

Suelen Gasparin[a,b*], Julien Berger[a], Rafik Belarbi[a], Denys Dutykh[c] and Nathan Mendes[d]

November 7, 2022

[a] LaSIE, UMR 7356 CNRS, La Rochelle University, Avenue Michel Crépeau, 17042 La Rochelle, France
[b] CEREMA, BPE Research Team, F-44000 Nantes, France
[c] LAMA, UMR 5127 CNRS, University Savoie Mont Blanc, Campus Scientifique 73376 Le Bourget du Lac, France
[d] LST, Mechanical Engineering Graduate Program, Pontifical Catholic University of Parana, Rua Imaculada Conceição, 1155, Curitiba, Brazil

*Corresponding author, e-mail address: suelen.gasparin@cerema.fr

Abstract

In this paper, the spectral method is developed as a reduced-order model for the solution of parametric problems within the building refurbishment framework. We propose to use the spectral reduced-order method to solve parametric problems in an innovative way, integrating the unknown parameter as one of the coordinates of the decomposition. The residual is minimized combining the Tau-Galerkin method with the Collocation approach. The developed method is evaluated in terms of accuracy and reduction of the computational time in three different cases. The dynamic behavior of unidimensional moisture diffusion is investigated. The cases focus on solving parametric problems in which the solution depends on space, time, diffusivity, and material thickness. Results highlight that the parametric spectral reduced-order method provides accurate solutions and can reduce ten times the degree of freedom of the solution. It allows efficient computation of the physical phenomena with a lower error when compared to traditional approaches.

keywords: Spectral methods; numerical simulation; reduced-order modeling; building renovation; parametric problems

1 Introduction

Most residential buildings in Europe were built before thermal regulations were introduced so that governments nowadays encourage their renovation to improve their energy efficiency. Nevertheless, the renovation of existing buildings can generate some moisture disorders if the renewal is not well planned. Therefore, to study building design, simulation tools can be used to estimate building energy consumption, thermal comfort, and moisture disorders regarding different retrofitting scenarios to propose efficient solutions [1].

In the context of thermal renovation, it is common to keep the original building envelope and add some insulation material on the inner/outer surface of the wall. To determine the optimum insulation to be applied to the building envelope refurbishment -in terms of material type, thickness and location-, hygrothermal simulations are needed in order to maximize energy efficiency and prevent moisture disorders [2].

To assess the hygrothermal performance and durability, moisture and heat transfers simulations must be performed for various retrofitting scenarios to find the best one. Thus, simulations are carried out for several parameter choices, such as orientation, diffusivity and thickness, which are called as *parametric solutions*. The challenge of a parametric problem is to solve the field of interest regarding several parameters, while the classic approach is to solve it for only space and time.

Several studies of parametric simulations regarding heat or moisture transfer are present in the literature. For example, in [3], the influence of wall thermal inertia on the energy consumption was investigated by using the `EnergyPlus` program for 24 construction types. In [4], the Moisture Buffer Value (MBV) of five hemp concrete materials were assessed using a numerical method. To perform studies regarding the optimum insulation thickness of a new insulation material in renovation of existing buildings, [5] performed several

simulations changing the length of the material to base their studies. However, since this kind of approach is computational costly, in [6] for example, they have chosen to simulate the dynamical thermal performance in multilayered walls for representative days. In [7] they chose to use a RC model to simplify the several simulations. In [8] they proposed the use of an innovative method to determine optimum insulation thickness based on non-uniform adaptive moving grid in order to reduced computational resources.

Despite the efforts to simplify the parametric problem with different approaches, they sill require large numbers of simulations. Indeed, the numerical model is not dependent on the parameters of interest. Thus, a computation of the numerical model is required for each value of the parameters within the domain of variation [9]. In addition, to assess moisture disorders, the horizon of simulation is of several years. Simulations of this type of problem demand considerable computational efforts and calculation time. In this way, instead of simulating the problem for each material and each thickness, we propose the use of a parametric solution to solve the problem only one time [10]. Therefore, a reduced-order model can be used to perform efficient parametric studies with reduced computational costs.

In the literature, some reduced-order models have been used to solve parametric problems in thermal building simulation. In [11] the authors have used the Proper Generalized Decomposition for the design of high energy performance building envelope. The reduction in the computation is hundred times if compared to some classical approaches. With the computational gain, other studies of parametric problems using reduced-order methods are found in the literature. In this way, in [12] they have combined the POD and PGD approach to modeling the soil for application in the study of canyon streets and in [13] to assess efficiently the building's envelope thermal performance.

Therefore, we propose to use a reduced-order model, based on Spectral methods as the one presented in [14] to solve parametric problems. It is based on the assumption of a separated form of the unknowns fields, and it has demonstrated its capabilities in dealing faster with high-dimensional problems [15]. The main advantage of the Spectral reduced-order model is the lower number of degrees of freedom needed to solve the problem if compared to conventional methods [16]. The Spectral approach assumes a separated tensorial representation of the solution by a finite sum of function products. It fixes a set of spatial basis functions to be the CHEBYSHEV polynomials, and then a system of ordinary differential equations is built to compute the temporal coefficients of the solution using the TAU–GALERKIN technique [17]. Regarding the parametric part, in this work it is proposed the use of the collocation approach to complement the problem.

Compared to the other parametric reduced methods presented in the literature, the spectral approach has the advantage of having a higher exponential convergence using less modes and being an *a priori* method using orthogonal polynomials as basis function [18]. This technique allows a different approach to deal with high dimensional problems. Problems like the parametric one can be solved into a multidimensional framework. The parameters in the model can be set as additional extra coordinates [19]. From the Spectral point of view, the resulting model is solved once, to obtain a general solution that includes all the solutions for every possible value of the parameters.

Thus, the scope of this work regards the development of the parametric Spectral reduced-order model technique to solve moisture diffusion problems, which has already been successfully implemented for simple diffusion problems [20]. The case studies are carried out regarding only the moisture transfer phenomena, assuming constant temperature. However, for future works it is important to also consider temperature variations since they are interdependent phenomena.

Hence, the paper is organized as follows: Section 2 presents the description of the physical phenomena. Then, Section 3 describes the Spectral reduced-order model technique. Then, three case studies are investigated: i) one-layer material wall with the moisture diffusivity as the third parameter (Section 4). Several features of the methods are analyzed in terms of both model order reduction and accuracy of the computed solution; ii) two-layer wall with the thickness as a third parameter (Section 5) and iii) practical case for renovation analysis considering climatic data including wind-driven rain (Section 6). To finalize, the Conclusion 7 is presented.

2 Mathematical formulation of the physical problem

For writing the mass conservation equation looking at obtaining a spectral reduced-order model for parametric analysis regarding moisture disorders, a macroscopic vision of the porous materials is considered, in which, hysteresis effect, temperature variations, chemical reactions and air movement are not taken in account.

2.1 The mass transport

Consider that a wall of thickness ℓ is composed of N material layers as depicted in Figure 1. For one dimensional problems, the spatial domain $x \in \Omega_x = [0, \ell]$ is defined as a composition of subdomains:

$$\Omega_x = \bigcup_{i=1}^{\mathsf{N}} \Omega_{x_i}, \qquad \text{where} \qquad x_i \in \Omega_{x_i} = [l_i, l_{i+1}], \qquad i = 1, 2, \ldots, \mathsf{N},$$

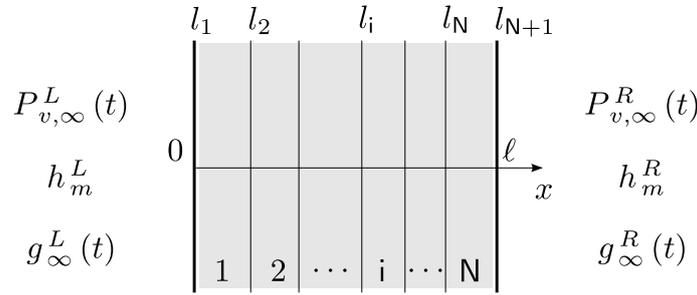with $l_1 = 0$ and $l_{\mathsf{N}+1} = \ell$.

Figure 1. Geometric configuration of the multi-layered wall.

The moisture flow occurs due to water diffusion in the vapor and liquid phases, according to FICK's and DARCY's laws. For practical applications, the mass conservation equation is written with the vapor pressure P_v [Pa] as the driving potential. It allows the continuity of the field and of the flow at the interface between materials [21]. Therefore, the mass conservation equation for each material layer $i = \{1, 2, \ldots, \mathsf{N}\}$ can be written as [22]:

$$c_{m,i} \frac{\partial P_{v,i}}{\partial t} = \nabla \cdot (k_{m,i} \nabla P_{v,i}), \tag{1}$$

with t [s] being the time, $c_{m,i}$ [kg/($\mathsf{m}^3 \cdot$ Pa)] being the moisture storage coefficient and $k_{m,i}$ [s] being the total moisture transfer coefficient. The transport coefficients are defined by:

$$c_{m,i} \stackrel{\text{def}}{:=} \frac{\partial w_i}{\partial \phi} \frac{1}{P_s}, \qquad\qquad k_{m,i} \stackrel{\text{def}}{:=} \delta_{v,i} + k_{l,i} \frac{\rho_l R_v T}{P_{v,i}},$$

where w_i [kg/m^3] is the volumetric moisture content of the material, ϕ [-] is the relative humidity, P_s [Pa] is the saturation pressure, $\delta_{v,i}$ [s] is the vapor permeability of the material, $k_{l,i}$ [s] is the liquid permeability of the material, ρ_l [kg/m^3] is the water density, R_v [J/(kg $\cdot$ K)] is the water vapor gas constant, and, T [K] is the temperature. The moisture content is a function of the relative humidity, *i.e.* $w : \phi \longmapsto w(\phi)$ which is obtained from material properties (sorption isotherm) and where the relative humidity ϕ is obtained from the relation:

$$\phi = \frac{P_v}{P_s}. \tag{2}$$

If, we assume that the transport coefficients $c_{m,i}$ and $k_{m,i}$ are positive constants then, the moisture transfer equation (1) can be written in a simplified way:

$$\frac{\partial P_{v,i}}{\partial t} = \nabla \cdot (\nu_{m,i} \nabla P_{v,i}), \tag{3}$$

where $\nu_{m,i} \stackrel{\text{def}}{:=} k_{m,i}/c_{m,i}$ [m^2/s] is the diffusivity coefficient.

2.1.1 Initial and boundary conditions

In order to well define the problem previously presented, the initial and boundary conditions must be set. For the initial condition, we consider a vapor pressure distribution as a function of the space:

$$P_{v,\mathsf{i}}\left(x_{\mathsf{i}},\, t\,=\,0\right)\;=\;P^0_{v,\mathsf{i}}\left(x_{\mathsf{i}}\right).$$

The moisture exchange between the environment and the wall surface is driven by vapor exchange, including evaporation, condensation, and driving rain:

$$k_{m,1}\,\frac{\partial P_{v,1}}{\partial x}\;=\;h^L_m\left(P_{v,1}-P^L_{v,\infty}\right)\,-\,g^L_\infty, \qquad\qquad \text{for } x=0,\; t\geqslant 0\,,$$

$$-\,k_{m,\mathsf{N}}\,\frac{\partial P_{v,\mathsf{N}}}{\partial x}\;=\;h^R_m\left(P_{v,\mathsf{N}}-P^R_{v,\infty}\right), \qquad\qquad \text{for } x=\ell,\; t\geqslant 0\,,$$

where $P_{v,\infty}$ [Pa] is the vapor pressure of the ambient air, h_m [s/m], is the convective moisture transfer coefficient, and g_∞ [kg/(m$^2\cdot$s)] is a source of liquid flow. If the bounding surface is in contact with the *outside* air, g_∞ will be the liquid flow from wind driven rain. The convective moisture transfer coefficient is constant in time $h_m\,=\,\text{const}>0$, and the ambient vapor pressure and the source therm vary with time:

$$P_{v,\infty}\;:\;t\;\longmapsto\;P_{v,\infty}\left(t\right), \qquad\qquad g_\infty\;:\;t\;\longmapsto\;g_\infty\left(t\right).$$

2.1.2 Interface between materials

The configuration assumed at the interface between materials follows the hydraulic continuity [23], which considers interpenetration of both porous structure layers. Consider two different materials, both of them are homogeneous and isotropic, and the moisture transfer is simulated through a perfectly airtight structure. The hydraulic continuity assumes that there is a continuous moisture distribution of vapor pressure:

$$P_{v,\mathsf{i}}\left(l_{\mathsf{i}+1},t\right)\;=\;P_{v,\mathsf{i}+1}\left(l_{\mathsf{i}+1},t\right), \tag{4}$$

and a continuous moisture flow across the interface:

$$\left(k_{m,\mathsf{i}}\,\frac{\partial P_{v,\,\mathsf{i}}}{\partial x}\right)\Bigg|_{x=l_{\mathsf{i}+1}}\;=\;\left(k_{m,\,\mathsf{i}+1}\,\frac{\partial P_{v,\,\mathsf{i}+1}}{\partial x}\right)\Bigg|_{x=l_{\mathsf{i}+1}}, \tag{5}$$

where $x=l_{\mathsf{i}+1}$ is the location of the interface between two materials.

2.2 Dimensionless formulation

Once the physical problem is posed, we can write its dimensionless formulation [24]. In this way, we define the following dimensionless quantity for the vapor pressure fields:

$$u_{\mathsf{i}}\;\overset{\text{def}}{:=}\;\frac{P_{v,\mathsf{i}}}{P_{v,\,\text{ref}}}\,,$$

where the subscript $\mathsf{i}\,=\,1,2,\dots,\mathsf{N}$ represents each material layer, the subscript **ref** represents a reference value, chosen according to the problem application. For the time and space, the dimensionless formulae are:

$$t^\star\;\overset{\text{def}}{:=}\;\frac{t}{t_{\,\text{ref}}}\,, \qquad\qquad x^\star_{\mathsf{i}}\;\overset{\text{def}}{:=}\;\frac{x-l_{\mathsf{i}}}{\beta_{\mathsf{i}}\,L_{\mathsf{i}}}\,,$$

where

$$L_{\mathsf{i}}\;=\;l_{\mathsf{i}+1}-l_{\mathsf{i}}\,, \qquad\qquad \beta_{\mathsf{i}}\in\mathbb{R}_{>0}\,,$$

in which the superscript * is a dimensionless quantity of the same variable and β_{i} is a positive constant related to the distortion of layer i. The distortion represents a dilatation regarding a reference value. This

way of written is chosen so β can appears in the dimensionless diffusive number and be parameterized. Moreover, the material properties are also scaled considering a reference value:

$$c_{m,\mathsf{i}}^{\star} \overset{\text{def}}{:=} \frac{c_{m,\mathsf{i}}}{c_{m,\,\text{ref}}}, \qquad\qquad k_{m,\mathsf{i}}^{\star} \overset{\text{def}}{:=} \frac{k_{m,\mathsf{i}}}{k_{m,\,\text{ref}}}.$$

In addition, we define ν, which is the equivalent of the FOURIER number that characterizes the importance of the mass transferred through the material:

$$\nu_{\mathsf{i}} \equiv \text{Fo} \overset{\text{def}}{:=} \frac{k_{m,\,\text{ref}}\, t_{\,\text{ref}}}{c_{m,\,\text{ref}}\, (\beta_{\mathsf{i}}\, L_{\mathsf{i}})^{\,2}}.$$

Therefore, the mass balance equation (1) for each layer can be written in a dimensionless form as:

$$c_{m,\mathsf{i}}^{\star} \frac{\partial u_{\mathsf{i}}}{\partial t^{\star}} = \nu_{\mathsf{i}} \frac{\partial}{\partial x_{\mathsf{i}}^{\star}} \left(k_{m,\mathsf{i}}^{\star} \frac{\partial u_{\mathsf{i}}}{\partial x_{\mathsf{i}}^{\star}} \right). \tag{6}$$

In the linear version, we consider $k_{m,\mathsf{i}} = k_{m,\,\text{ref}}$ and $c_{m,\mathsf{i}} = c_{m,\,\text{ref}}$ which leads to a simplified expression:

$$\frac{\partial u_{\mathsf{i}}}{\partial t^{\star}} = \nu_{\mathsf{i}} \frac{\partial^2 u_{\mathsf{i}}}{\partial x_{\mathsf{i}}^{\star\, 2}}. \tag{7}$$

At the boundaries, we have Bi_m as the mass transfer BIOT number and $g_{\infty}^{\star}$ as the dimensionless representation of the source terms at the boundaries:

$$\text{Bi}_m^L \overset{\text{def}}{:=} \frac{h_m^L\, (\beta_1\, L_1)}{k_{m,\,\text{ref}}}, \qquad \text{Bi}_m^R \overset{\text{def}}{:=} \frac{h_m^R\, (\beta_{\mathsf{N}}\, L_{\mathsf{N}})}{k_{m,\,\text{ref}}}, \qquad g_{\infty}^{\star L} \overset{\text{def}}{:=} \frac{g_{\infty}^L\, (\beta_1\, L_1)}{k_{m,\,\text{ref}}\, P_{v,\,\text{ref}}},$$

which leads to the dimensionless formulation of the boundary conditions:

$$k_{m,1}^{\star} \left. \frac{\partial u_1}{\partial x_1^{\star}} \right|_{x_1^{\star}=0} = \text{Bi}_m^L \left(u_1 - u_{\infty}^L \right) - g_{\infty}^{\star L}, \tag{8}$$

$$- k_{m,\mathsf{N}}^{\star} \left. \frac{\partial u_{\mathsf{N}}}{\partial x_{\mathsf{N}}^{\star}} \right|_{x_{\mathsf{N}}^{\star}=1} = \text{Bi}_m^R \left(u_{\mathsf{N}} - u_{\infty}^R \right), \tag{9}$$

and of the initial conditions as:

$$u_{\mathsf{i}}\, (x_{\mathsf{i}}^{\star}, t^{\star} = 0) = u_{\mathsf{i}}^0\, (x_{\mathsf{i}}^{\star}).$$

The interface conditions in the dimensionless form are written as:

$$u_{\mathsf{i}}\, (x_{\mathsf{i}}^{\star} = 1, t^{\star}) = u_{\mathsf{i}+1}\, (x_{\mathsf{i}+1}^{\star} = 0, t^{\star}), \tag{10a}$$

$$\left. \frac{\partial u_{\mathsf{i}}}{\partial x_{\mathsf{i}}^{\star}} \right|_{x_{\mathsf{i}}^{\star}=1} = \kappa_{\mathsf{i}+1} \left. \frac{\partial u_{\mathsf{i}+1}}{\partial x_{\mathsf{i}+1}^{\star}} \right|_{x_{\mathsf{i}+1}^{\star}=0}, \tag{10b}$$

where κ represents the interface exchange coefficient between two layers:

$$\kappa_{\mathsf{i}+1} = \frac{k_{m,\mathsf{i}+1}}{k_{m,\mathsf{i}}} \frac{\beta_{\mathsf{i}}\, L_{\mathsf{i}}}{\beta_{\mathsf{i}+1}\, L_{\mathsf{i}+1}}.$$

2.3 Metrics of model efficiency

2.3.1 Error

To analyse the accuracy of the methods, the error between the simulated solution $Y^{\,\mathrm{num}}$, and the reference solution $Y^{\,\mathrm{ref}}$, are computed as functions of x using the following EUCLIDEAN norm:

$$\varepsilon_2\left(x_{\mathsf{i}}^{\star},\,\nu\right) \;\overset{\mathrm{def}}{:=}\; \sqrt{\frac{1}{\mathrm{N}_t}\sum_{\mathsf{j}=1}^{\mathrm{N}_t}\left(Y_{\mathsf{j}}^{\,\mathrm{num}}\left(x_{\mathsf{i}}^{\star},\,t_{\mathsf{j}}^{\star},\,\nu\right)\;-\;Y_{\mathsf{j}}^{\,\mathrm{ref}}\left(x_{\mathsf{i}}^{\star},\,t_{\mathsf{j}}^{\star},\,\nu\right)\right)^2}\,,$$

where N_t is the number of temporal steps and $Y^{\,\mathrm{num}}$ is the field of interest. The reference solution $Y^{\,\mathrm{ref}}$ is computed using the `Matlab`$^{\mathrm{TM}}$ open source toolbox `Chebfun` [25]. Moreover, the uniform norm error ε_∞ is given by the maximal values of ε_2:

$$\varepsilon_\infty\left(\nu\right) \;\overset{\mathrm{def}}{:=}\; \sup_{x_{\mathsf{i}}^{\star}\,\in\,\left[\,0,1\,\right]}\varepsilon_2\left(x_{\mathsf{i}}^{\star},\,\nu\right).$$

In addition, we introduce the error $\varepsilon_{\infty,\nu}$ regarding the parametric error analysis:

$$\varepsilon_{\infty,\,\nu} \;\overset{\mathrm{def}}{:=}\; \max_{\Omega_\nu}\varepsilon_\infty\left(\nu\right).$$

The lower the error value, the better the method is able to fit the physical model. Since we are working with dimensionless values, we state that if the error is above the maximum limit of $\varepsilon\leqslant 10^{-2}$, the solution provided by the numerical scheme is not considered to be accurate enough. This means, an accuracy of two decimal digits [26].

2.3.2 Computational time

Another criterion of evaluation is the computational (CPU) time $t_{\mathrm{cpu}}\,[\mathsf{s}]$ spent by the numerical model to compute the solution. The measurement is carried out using the `Matlab`$^{\mathrm{TM}}$ platform and a computer with a processor Intel®Core$^{\mathrm{TM}}$i5 @ 2.80GHz×4 and 16GB of RAM. The ratio $\mathrm{R}_{\mathrm{cpu}}$ is defined by:

$$\mathrm{R}_{\mathrm{cpu}} \;\overset{\mathrm{def}}{:=}\; \frac{t_{\mathrm{cpu}}}{t_\circ}\,,$$

where $t_\circ$ is a reference time. One should notice that the codes are not optimized, and the slight differences between the CPU time should not be considered.

3 The Parametric Spectral Reduced-Order Model

In one-dimensional diffusion problems, the field within the material is normally calculated with time and space being the independent variables, while the diffusivity, the specific capacity, and the thickness of the material are parameters of the problem. Here, a parametric problem considers one of these parameters as also being an independent variable. Thus, the solution is computed depending on the time and space coordinates and also depending on an extra parameter ν of the problem. In this case, the field is computed considering *three* independent variables, different from the classical approach:

$$\begin{array}{ll}\text{Traditional} & \text{Parametric-SROM}\\[4pt] u:\;(x^{\star},t^{\star})\;\longmapsto\;u\,(x^{\star},t^{\star})\,, & u:\;(x^{\star},t^{\star},\nu)\;\longmapsto\;u\,(x^{\star},t^{\star},\nu)\,.\end{array}$$

Hence, the solution is sought as $u\,(x^{\star},\,t^{\star},\,\nu)$, where ν is defined as a coordinate of the problem. Instead of solving the diffusion equation for each value of the new variable in a loop, the proposed approach considers the new independent variable as a new dimension as represented in Figure 2.
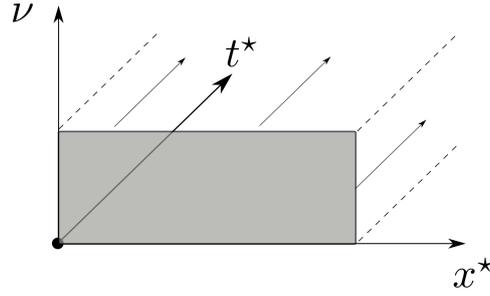
Figure 2. Representation of the Parametric-SROM solution.

Considering the linear diffusion equation (7) we have $t^\star \in [0, \tau]$ and $x^\star \in [0, 1]$. The third coordinate is within $\nu \in [\nu_{\min}, \nu_{\max}]$. Thus, instead of propagate a solution in time for a fixed ν, we propagate a family of solutions that are parametrized by ν, as illustrated in Figure 2. It is almost like solving three-dimensional problems $(x^\star, t^\star, \nu)$. The difference is that there is no partial derivative regarding the third parameter in Equation (6). Therefore, we seek for a solution of u that depends on three parameters:

$$u : (x^\star, t^\star, \nu) \in [0, 1] \times [0, \tau] \times [\nu_{\min}, \nu_{\max}] \longmapsto \mathbb{R}.$$

where ν is a mapping allowing the parametrization of the Eqution according to the transfer coefficient, the storage coefficient, the diffusivity coefficient, the reference time or the material thickness:

$$\nu : \left(k_{m, \text{ref}}; c_{m, \text{ref}}; t_{\text{ref}}; \beta_{\mathsf{i}}\right) \in \mathbb{R}^4 \longmapsto \mathbb{R},$$

For a direct solution, the use of the reduced-order method based on the spectral approach is proposed due to its high computation efficiency [20].

3.1 The parametric spectral approach

Before applying the spectral method, the intervals $\nu \in [\nu_{\min}, \nu_{\max}]$ and $x^\star \in [0, 1]$ must be transformed to the canonical one $[-1, 1]$. The description of the transformation can be found in the Appendix A.1 for the spatial domain and in Appendix A.2 for the parametric domain. Thus, $\bar{\nu}$ and $\bar{x}$ represents the following transformations:

$$[\nu_{\min}, \nu_{\max}] \xrightarrow{\bar{\nu}} [-1, 1], \qquad\qquad [0, 1] \xrightarrow{\bar{x}} [-1, 1].$$

The Spectral method assumes that the unknown u, which depends on $(\bar{x}, t^\star, \bar{\nu})$, can be accurately represented as a finite sum:

$$u(\bar{x}, t^\star, \bar{\nu}) \approx u_{nm}(\bar{x}, t^\star, \bar{\nu}) = \sum_{i=1}^{n} \sum_{j=1}^{m} a_{ij}(t^\star) \mathsf{T}_{i-1}(\bar{x}) \mathsf{P}_{j-1}(\bar{\nu}). \tag{11}$$

Here, $\{\mathsf{T}_{i-1}(\bar{x})\}_{i=1}^{n}$ and $\{\mathsf{P}_{j-1}(\bar{\nu})\}_{j=1}^{m}$ are the sets of basis functions, $\{a_{ij}(t^\star)\}_{i,j=1}^{n,m}$ are the corresponding time-dependent spectral coefficients and $n \cdot m$ represents the number of degrees of freedom of the solution. Equation (11) can be seen as a series truncation after $N = n$ and $M = n$ modes. The CHEBYSHEV polynomials are chosen for the spatial basis functions and for the parametric basis functions.

Using the recursive expression of the derivatives [27], the residual of Equation (6) is given by:

$$R(\bar{x}, t^\star, \bar{\nu}) = \sum_{i=1}^{n} \sum_{j=1}^{m} \left[\dot{a}_{ij}(t^\star) - \nu \tilde{\tilde{a}}_{ij}(t^\star)\right] \mathsf{T}_{i-1}(\bar{x}) \mathsf{P}_{j-1}(\bar{\nu}), \tag{12}$$

where $\dot{a} \overset{\text{def}}{:=} \dfrac{\partial a}{\partial t^\star}$ according to NEWTON's notation and coefficients $\{\tilde{a}_{ij}(t^\star)\}_{i,j=1}^{n,m}$ and $\{\tilde{\tilde{a}}_{ij}(t^\star)\}_{i,j=1}^{n,m}$ are re-expressed in terms of coefficients $\{a_{ij}(t^\star)\}_{i,j=1}^{n,m}$. The purpose is to minimize the residual:

$$\left\| R(\bar{x}, t^\star, \bar{\nu}) \right\|_2 \longrightarrow \min,$$

which is performed via two methods, the TAU–GALERKIN and the Pseudospectral method. For this, the residual, Equation (12), is required to be orthogonal to the CHEBYSHEV basis functions $\langle R, \mathsf{T}_k \rangle = 0$ at the collocation points $\bar{\nu}_p$:

$$\langle R, \mathsf{T}_k \rangle = \int_{-1}^1 \frac{R(\bar{x}, t^\star, \bar{\nu}_p) \, \mathsf{T}_k(\bar{x})}{\sqrt{1 - \bar{x}^2}} \, \mathrm{d}\bar{x} = 0,$$

with,

$$k = 0, 1, 2, \ldots, n-2, \qquad \text{and} \qquad p = 1, 2, \ldots, m.$$

The collocation points of the CHEBYSEHEV polynomials most used in the literature are the extrema points [27]. In Section 4.2 the selection of the collocations points is discussed in more details.

As a result, the projected residual can be written as:

$$\sum_{i=1}^n \sum_{j=1}^m \underbrace{\dot{a}_{ij}(t^\star)}_{\dot{\mathsf{A}}} \underbrace{\mathsf{P}_{j-1}(\bar{\nu}_p) \int_{-1}^1 \frac{\mathsf{T}_{i-1}(\bar{x})\mathsf{T}_k(\bar{x})}{\sqrt{1 - \bar{x}^2}}\mathrm{d}\bar{x}}_{\mathcal{M}} = \underbrace{\sum_{i=1}^n \sum_{j=1}^m \nu_p \tilde{a}_{ij}(t^\star) \mathsf{P}_{j-1}(\bar{\nu}_p) \int_{-1}^1 \frac{\mathsf{T}_{i-1}(\bar{x}) \, \mathsf{T}_k(\bar{x})}{\sqrt{1 - \bar{x}^2}}\mathrm{d}\bar{x}}_{\mathsf{G}}. \quad (13)$$

Equation (13) gives $(n-2) \cdot m$ equations. The extra coefficients are obtained by substituting the decomposed solution into the equations (9) of the boundary conditions:

$$b_{(n-1)\cdot p} = \sum_{i=1}^n \sum_{j=1}^m \tilde{a}_{ij}(t^\star) \, \mathsf{T}_{i-1}(-1) \, \mathsf{P}_{j-1}(\bar{\nu}_p) - \mathrm{Bi}_{m,p}^L \left[\sum_{i=1}^n \sum_{j=1}^m a_{ij}(t^\star) \, \mathsf{T}_{i-1}(-1) \, \mathsf{P}_{j-1}(\bar{\nu}_p) + u_\infty^L(t^\star) \right] + g_\infty^{\star L}(t^\star), \quad (14a)$$

$$b_{n\cdot p} = - \sum_{i=1}^n \sum_{j=1}^m \tilde{a}_{ij}(t^\star) \, \mathsf{T}_{i-1}(1) \, \mathsf{P}_{j-1}(\bar{\nu}_p) - \mathrm{Bi}_{m,p}^R \left[\sum_{i=1}^n \sum_{j=1}^m a_{ij}(t^\star) \, \mathsf{T}_{i-1}(1) \, \mathsf{P}_{j-1}(\bar{\nu}_p) + u_\infty^R(t^\star) \right], \quad (14b)$$

with $T_i(-1) = (-1)^i$ and $T_i(1) \equiv 1$ [17]. Equations (14a) and (14b) supplies $2 \cdot m$ equations in a system of $n \cdot m$ equations.

The matrix of spectral coefficients $\{a_{ij}\}_{i,j=1}^{n,m}$ is transformed into a vector $a_{ij} \longmapsto a_{l = (i-1)n+j}$ to simplify calculations:

$$\mathsf{A}_{ij} = \left[a_{11}, a_{12}, \ldots, a_{1n}, a_{21}, a_{22}, \ldots, a_{2n}, a_{m1}, a_{m2}, \ldots, a_{mn} \right]^\top,$$

with $\mathsf{A} \in \mathbb{R}^{mn}$ being the vector transformation. In this way, it is possible to compose the reduced system of ODEs to be solved plus the two additional algebraic expressions regarding the boundary conditions. Finally, the system of Differential-Algebraic Equations (DAEs) has the following form:

$$\mathcal{M} \, \dot{\mathsf{A}}_{ij}(t^\star) = \mathsf{G}(t^\star, \mathsf{A}_{ij}) + \mathsf{b}(t^\star, \mathsf{A}_{ij}), \quad (15)$$

where, $\mathcal{M} \in \mathrm{Mat}_{nm \times nm}(\mathbb{R})$ is the mass matrix, $\mathsf{G} \in \mathbb{R}^{nm}$ is a vector containing the second derivative relation, and $\mathsf{b} \in \mathbb{R}^{nm}$ is a vector containing the elements b_{n-1} and b_n of the boundary conditions:

$$\mathsf{b} = \left[0, 0, \cdots, b_{(n-1)\cdot 1}, b_{n\cdot 1}, \cdots, 0, 0, \cdots, b_{(n-1)\cdot p}, b_{n\cdot p} \right]^\top.$$

Initial values of the coefficients $\{a_{ij}(t^\star = 0)\}$ are calculated by the projection of the initial condition [28]:

$$a_0 \approx a_{ij}(0) = \frac{2}{\pi \, c_k} \int_{-1}^1 \frac{u_0(\bar{x}) \, \mathsf{T}_k(\bar{x})}{\sqrt{1 - \bar{x}^2}} \, \mathrm{d}\bar{x}, \qquad k = 0, 1, \ldots, n-2, \quad (16)$$

where, $u_0(\bar{x})$ is the dimensionless initial condition. Thus, by using the Spectral reduced-order model approach to build the reduced-order model, the time-dependent coefficients $\{a_i(t^\star)\}_{i,j=1}^{n,m}$ are computed by solving the following system:

$$\begin{cases} \mathcal{M} \, \dot{\mathsf{A}}_{ij}(t^\star) &= \mathsf{G}(t^\star, \mathsf{A}_{ij}) + \mathsf{b}(t^\star, \mathsf{A}_{ij}) \\ \mathsf{A}_{ij}(0) &= \mathsf{A}_0, \end{cases} \quad (17)$$

where $A_0 = \mathbf{Id} \otimes a_0$, $\mathbf{Id}$ is the identity matrix of size $\mathrm{Mat}_{m \times m}(\mathbb{R})$ and the operation denoted by $\otimes$ is the KRONECKER product [29]. The main advantage of a Spectral-ROM is that the number of degrees of freedom needed to solve the diffusion problem (6) is much lower than the ones needed in conventional methods such as finite differences [20].

Different approaches can be used to solve the ODE system (17). In this work, we apply a numerical integration scheme, *e.g.* an adaptative RUNGE–KUTTA with moderate accuracy, since problem (17) is just a reduced-order model. So, with embedded error control and not so stringent tolerances, it can be solved very efficiently. In this study, we shall employ ODE solvers since we are interested in the whole trajectory. After solving the *reduced* system of ODEs, it is possible to compose the solution along with the CHEBYSHEV polynomial.

3.2 Extension to multilayered domains

Consider a wall composed of two material layers as presented in Figure 3(a). The spatial domain is composed of two sub-domains $\Omega_{x_1^\star} = [0, 1]$ and $\Omega_{x_2^\star} = [0, 1]$. Before applying the spectral approach, the spatial domains need to be transformed to the canonical one $[-1, 1]$. For this reason, $\Omega_{x_1^\star}$ and $\Omega_{x_2^\star}$ are linearly transformed to the spectral domains $\Omega_{\bar{x}_1}$ and $\Omega_{\bar{x}_2}$, as illustrated in Figure 3, so they can fit within the interval of interest. In addition ν is also transformed to the canonical interval $[\nu_{\min}, \nu_{\max}] \xrightarrow{\bar{\nu}} [-1, 1]$.

(a) Dimensionless domain
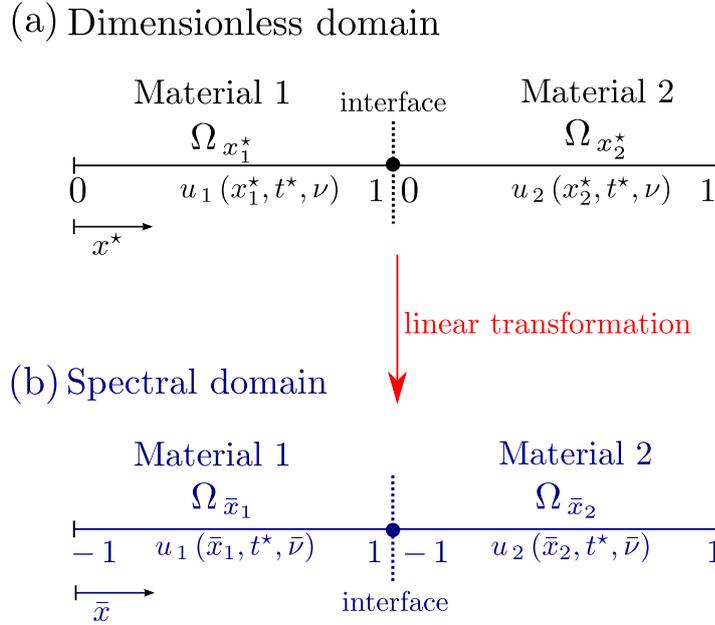

(b) Spectral domain

Figure 3. Schematic representation of the domain division with the real domain (a) transformed linearly to obtain the spectral domain (b).

Therefore, u_1 and u_2 are approximated by the sums:

$$u_1(\bar{x}, t^\star, \bar{\nu}) = \sum_{i=1}^{n} \sum_{j=1}^{m} a_{1,ij}(t^\star) \, \mathsf{T}_{i-1}(\bar{x}) \, \mathsf{P}_{j-1}(\bar{\nu}),$$

$$u_2(\bar{x}, t^\star, \bar{\nu}) = \sum_{i=1}^{n} \sum_{j=1}^{m} a_{2,ij}(t^\star) \, \mathsf{T}_{i-1}(\bar{x}) \, \mathsf{P}_{j-1}(\bar{\nu}).$$

The condition at the interface between the two materials states the continuity of the fields and the flows as in Equation (10). It implies that the derivatives of the field u is not continuous at the interface. This important remark has to be taken into account in the construction of the spectral reduced-order model. Indeed, the domain is decomposed into subdomains to maintain a smooth solution. In this way, the reduced-order

model is optimal and ensures the error of the Spectral-ROM decreases exponentially. It is possible to build the reduced-order model considering the whole domain (without decomposition). However, the convergence would be undermined since the solution and its derivatives are not smooth at the interface and we cannot impose the desired conditions.

The residual is required to be orthogonal to the CHEBYSHEV basis functions $\langle R, \mathsf{T}_k \rangle = 0$ at the collocation points $\bar{\nu}_p$, as described in Section 3, which leads to:

$$\sum_{i=1}^{n}\sum_{j=1}^{m} \dot{a}_{1,ij}(t^\star) \underbrace{\mathsf{P}_{j-1}(\bar{\nu}_p) \int_{-1}^{1} \frac{\mathsf{T}_{i-1}(\bar{x})\,\mathsf{T}_k(\bar{x})}{\sqrt{1-\bar{x}^2}}\mathrm{d}\bar{x}}_{\mathcal{M}} = \underbrace{\mathrm{Fo}_{1,p}\sum_{i=1}^{n}\sum_{j=1}^{m} \tilde{\tilde{a}}_{1,ij}(t^\star)\,\mathsf{P}_{j-1}(\bar{\nu}_p)\int_{-1}^{1}\frac{\mathsf{T}_{i-1}(\bar{x})\,\mathsf{T}_k(\bar{x})}{\sqrt{1-\bar{x}^2}}\mathrm{d}\bar{x}}_{\mathrm{G}_1}, \qquad (18)$$

$$\sum_{i=1}^{n}\sum_{j=1}^{m} \dot{a}_{2,ij}(t^\star) \underbrace{\mathsf{P}_{j-1}(\bar{\nu}_p) \int_{-1}^{1} \frac{\mathsf{T}_{i-1}(\bar{x})\,\mathsf{T}_k(x)}{\sqrt{1-\bar{x}^2}}\mathrm{d}\bar{x}}_{\mathcal{M}} = \underbrace{\mathrm{Fo}_{2,p}\sum_{i=1}^{n}\sum_{j=1}^{m} \tilde{\tilde{a}}_{2,ij}(t^\star)\,\mathsf{P}_{j-1}(\bar{\nu}_p)\int_{-1}^{1}\frac{\mathsf{T}_{i-1}(\bar{x})\,\mathsf{T}_k(\bar{x})}{\sqrt{1-\bar{x}^2}}\mathrm{d}\bar{x}}_{\mathrm{G}_2}, \qquad (19)$$

with,

$$k = 0, 1, 2, \ldots, n-2, \qquad \text{and} \qquad p = 1, 2, \ldots, m.$$

The interface conditions represented in Equation (10) are then written in the spectral form as:

$$b_{1,(n-1)\cdot p} = \sum_{i=1}^{n}\sum_{j=1}^{m} a_{1,ij}(t^\star)\,\mathsf{T}_{i-1}(+1)\,\mathsf{P}_{j-1}(\bar{\nu}_p) - \sum_{i=1}^{n}\sum_{j=1}^{m} a_{2,ij}(t^\star)\,\mathsf{T}_{i-1}(-1)\,\mathsf{P}_{j-1}(\bar{\nu}_p),$$

$$b_{1,n\cdot p} = k_{m,1}^\star\sum_{i=1}^{n}\sum_{j=1}^{m} \tilde{a}_{1,ij}(t^\star)\,\mathsf{T}_{i-1}(+1)\,\mathsf{P}_{j-1}(\bar{\nu}_p) - k_{m,2}^\star\sum_{i=1}^{n}\sum_{j=1}^{m} \tilde{a}_{2,ij}(t^\star)\,\mathsf{T}_{i-1}(-1)\,\mathsf{P}_{j-1}(\bar{\nu}_p),$$

which are included in the vector b_1. In the same way, the boundary conditions are written in the spectral form as:

$$b_{2,(n-1)\cdot p} = k_{m,1}^\star\sum_{i=1}^{n}\sum_{j=1}^{m} \tilde{a}_{1,ij}(t^\star)\,\mathsf{T}_{i-1}(-1)\,\mathsf{P}_{j-1}(\bar{\nu}_p) + \mathrm{Bi}_p^L\left[\sum_{i=1}^{n}\sum_{j=1}^{m} a_{1,ij}(t^\star)\,\mathsf{T}_{i-1}(-1)\,\mathsf{P}_{j-1}(\bar{\nu}_p) + u_\infty^L\right],$$

$$b_{2,n\cdot p} = k_{m,2}^\star\sum_{i=1}^{n}\sum_{j=1}^{m} \tilde{a}_{2,ij}(t^\star)\,\mathsf{T}_{i-1}(+1)\,\mathsf{P}_{j-1}(\bar{\nu}_p) - \mathrm{Bi}_p^R\left[\sum_{i=1}^{n}\sum_{j=1}^{m} a_{2,ij}(t^\star)\,\mathsf{T}_{i-1}(+1)\,\mathsf{P}_{j-1}(\bar{\nu}_p) + u_\infty^R\right],$$

and are included in b_2. Vectors b_1 and b_2 are $n \cdot m \times 1$ column vectors with the form:

$$b_1 = \left[0, 0, \cdots, b_{1,(n-1)\cdot 1}, b_{1,n\cdot 1}, \cdots, 0, 0, \cdots, b_{1,(n-1)\cdot p}, b_{1,n\cdot p}\right]^\top,$$

$$b_2 = \left[0, 0, \cdots, b_{2,(n-1)\cdot 1}, b_{2,n\cdot 1}, \cdots, 0, 0, \cdots, b_{2,(n-1)\cdot p}, b_{2,n\cdot p}\right]^\top.$$

Therefore, the differential-algebraic system considering both materials becomes:

$$\begin{pmatrix} \mathcal{M} & \mathbf{0} \\ \mathbf{0} & \mathcal{M} \end{pmatrix} \cdot \begin{bmatrix} \dot{\mathrm{A}}_{1,ij} \\ \dot{\mathrm{A}}_{2,ij} \end{bmatrix} = \begin{bmatrix} \mathrm{G}_1 \\ \mathrm{G}_2 \end{bmatrix} + \begin{bmatrix} b_1 \\ b_2 \end{bmatrix}.$$

With all elements listed before, it is possible to set the system to be solved. The system of ODEs for solving the parametric problem of moisture transfer with two layers has the size of $2 \cdot n \cdot m$ with $2 \cdot n$ additional algebraic expressions for the interface conditions. The initial condition is also given by Equation (16) and the DAE system is solved by the Matlab™ solver ODE15s. In this work, the approach was presented for a two-layered wall for the sake of clarity, knowing it can be easily extended to any number of layers and any other boundary condition at their interfaces.

4 Parametric problem regarding the diffusivity

Here, the parametric problem is solved regarding the time t, the space x and the moisture diffusivity coefficient ν_m. Thus, the family of solutions sought are:

$$P_v \;:\; \mathcal{I}_x \times \mathcal{I}_t \times \mathcal{I}_{k_m} \times \mathcal{I}_{c_m} \;\longrightarrow\; \mathbb{R}\,,$$
$$(x,\, t,\, k_m,\, c_m) \;\longmapsto\; P_v\,(x,\, t, \nu)\,,$$

where $\nu : (\, k_m,\, c_m \,) \longmapsto \nu = \frac{k_{m,\,\mathrm{ref}}\, t_{\,\mathrm{ref}}}{c_{m,\,\mathrm{ref}}\,(\beta\, L)^2}$ is defined as a coordinate of the problem within a given interval $\nu \in \mathcal{I}_\nu \equiv [\,\nu_{\min},\, \nu_{\max}\,]$, in which β, L, $t_{\,\mathrm{ref}}$ fixed as constants so ν enables to build a material diffusivity $\nu = \dfrac{k_m}{c_m}$ parametric solution. In addition, we introduce N_ν that is noted as the number of elements (the cardinal) of the domain. By making the ν vary we are actually working with the variations of the conductivity k_m and capacity c_m as indicated in Figure 4. Thus, by using the dimensionless formulation the only value that varies is the ν number:

$$\nu \;:\; [c_{m,\min},\, c_{m,\max}] \times [k_{m,\min},\, k_{m,\max}] \;\longrightarrow\; [\nu_{\min},\, \nu_{\max}]$$

Figure 4. Mapping of the parametric problem regarding the diffusivity.

Two approaches are adopted to solve this problem. The first one is by computing the solution $P_v\,(x,\, t)$ for each value of the parameter ν, by means of a loop in the algorithm. The second option is by computing the solution as a decomposition on each coordinate of the problem as presented in Section 3.

In the sequence we present a parametric case study regarding the moisture diffusivity. First, the descrption of the case is given and then the results are discussed. In addition, this case is also used to evaluate the *numerical features* of the Parametric-SROM approach and also the *the computational cost.*

4.1 Description of the case study

For this case, we seek for a parametric solution of Equation (1). The vapor pressure is computed as a function of time t, space x and the moisture diffusivity of different materials. The left boundary is exposed to cyclic changes of relative humidity between $33\,\%$ and $75\,\%$, with a $24\,\mathrm{h}$ period as presented in Figure 5. The total time of simulation is four days, the equivalent to $96\,\mathrm{h}$. The convective vapor transfer coefficient is set to $h_v = 2 \cdot 10^{-8}\,\mathrm{s/m}$. The right boundary is set impermeable. The initial condition is homogeneous among all materials with a vapor pressure value of $P_{v,\mathrm{i}} = 925.46\,\mathrm{Pa}$, being the equivalent to a relative humidity of $33\,\%$. Simulations undergo at a constant $23°\mathrm{C}$ temperature that leads to a saturation pressure of $2804.4\,\mathrm{Pa}$. All materials have the same 10-cm thickness with the properties given in Table 1. The transfer coefficient considers only vapor transport, which leads to the moisture diffusivity varying within $\Omega_{nu} = [1.97 \cdot 10^{-10},\, 2.19 \cdot 10^{-8}]\,\mathrm{m^2/s}$. This case study is inspired in the one presented by [30], including the material properties, to study the so-called moisture buffer effects.
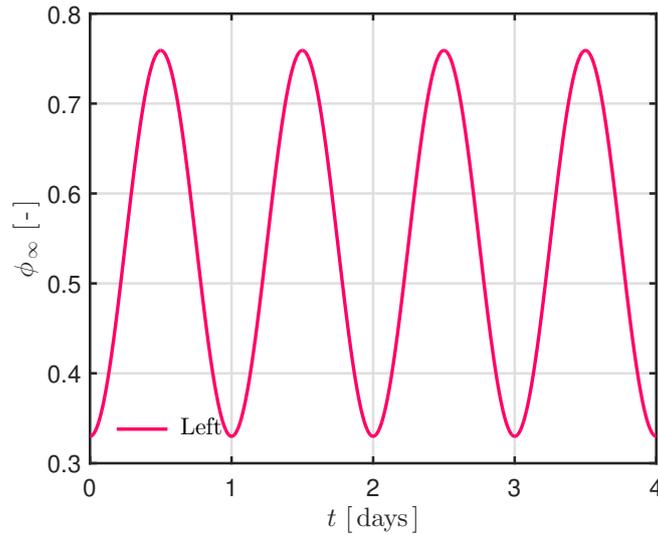
Figure 5. Evolution of the relative humidity at the left boundary on the parametric case.

Material	*Storage coefficient* c_m [kg/(m³.Pa)]	*Transfer coefficient* k_m [s]	*Diffusivity* ν [m²/s]
Aggregate concrete	$5.08 \cdot 10^{-2}$	$1 \cdot 10^{-11}$	$\nu_1 = 1.97 \cdot 10^{-10}$
Birch panel	$3.57 \cdot 10^{-2}$	$1.5 \cdot 10^{-11}$	$\nu_2 = 4.21 \cdot 10^{-10}$
Spruce board	$2.92 \cdot 10^{-2}$	$1.5 \cdot 10^{-11}$	$\nu_3 = 5.14 \cdot 10^{-10}$
Gypsum	$1.11 \cdot 10^{-2}$	$2.5 \cdot 10^{-11}$	$\nu_4 = 2.26 \cdot 10^{-9}$
Cellular concrete	$1.27 \cdot 10^{-2}$	$7 \cdot 10^{-11}$	$\nu_5 = 5.50 \cdot 10^{-9}$
Brick	$1.37 \cdot 10^{-3}$	$3 \cdot 10^{-11}$	$\nu_6 = 2.19 \cdot 10^{-8}$

Table 1. Properties of the materials used in the parametric case [31].

4.2 Results and discussion

Simulations are performed for 6 different values of moisture diffusivity coefficients in the segment $\mathcal{I}_\nu$, representing the materials of Table 1. The Parametric-SROM model is compared with the Euler-implicit scheme, with the Spectral method using a loop over the parameter values and also with the reference solution, obtained with the `Chebfun` toolbox.

Figure 6(a) shows the profiles of vapor pressure within each material at the time instant $t = 48\,\text{h}$. It is possible to observe significant variations of the vapor pressure within each material as the value of the moisture diffusivity coefficient increases. Furthermore, Figure 6(b) presents the evolution of vapor pressure near the left boundary, at $x = 1\,\text{cm}$. In these figures, the Parametric-SROM approach is in a good agreement with the reference solution, with a maximum error on the order of 10^{-3}. However, some oscillations can be observed in Figure 6(a) only for ν_1. This occurs because the diffusivity coefficient is very low and the number of modes was not enough to support the stiffness of the problem. This problem can be avoided by implementing a system of an automatic increase in the number of modes but it can increase the computational cost if not well designed. It is one of the perspectives of continuation of this work.

In addition, with the simulated solution, it is possible to verify the variation of moisture content in each material. For this, Figure 7 presents the moisture content in grams of water per kilogram of material, over the time. As the materials are hygroscopically different, the approach can also be tested on the determination of Moisture Buffer Values (MBV). The material of the curve on the graphic corresponding to $\nu_{\min}$ retains very low quantity of mass while the material of $\nu_{\max}$ accumulates more the moisture according to the increase of ambient relative humidity.

To perform the parametric simulation, the Parametric-SROM needed around $N = 19$ modes for the
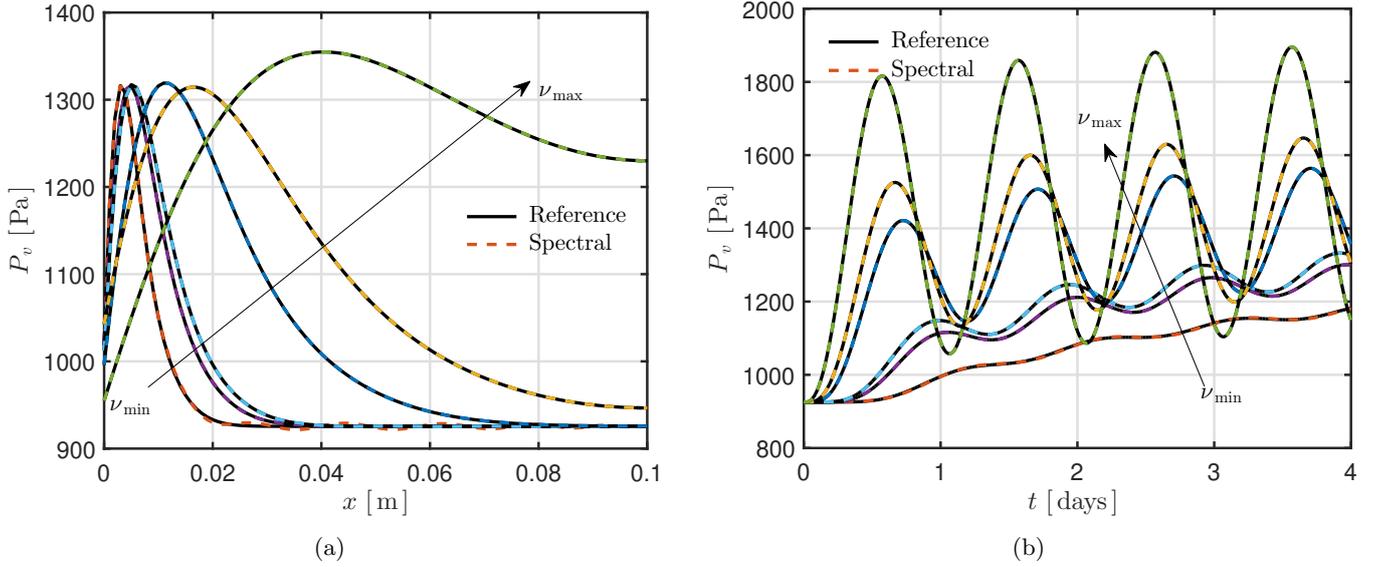
Figure 6. Vapor pressure profiles for each one of the materials at the time instant of $t = 48\,\text{h}$ (a) and the vapor pressure evolution near the left boundary at $x = 1\,\text{cm}$ (b).
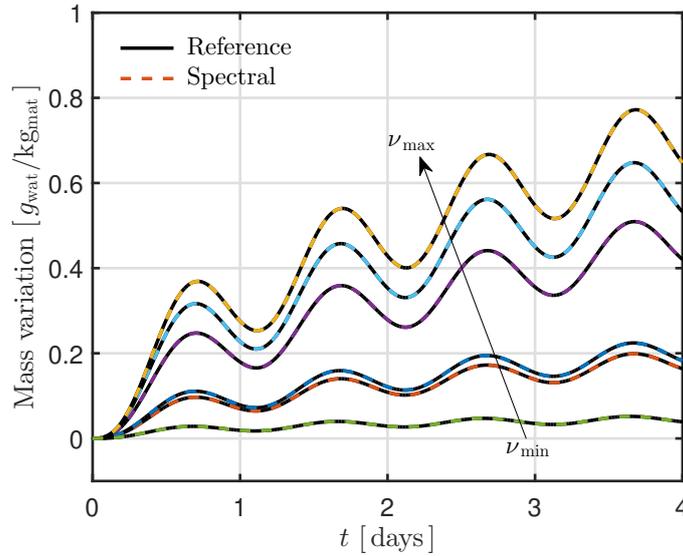

Figure 7. Evolution of the mass variation of each material.

spatial base functions and $M = 6$ modes for the parametric base functions, with the tolerance of the solver `ode15s` set to $\text{tol} = 10^{-5}$. The solution is projected on a grid composed by $\Delta \bar{x} = 1 \cdot 10^{-2}$ and $\Delta \bar{t} = 1 \cdot 10^{-2}$. The time step of solver `ode15s` is adaptive, but we can choose to have the output in the time step we want. The solver will integrate the solution with its time step and then give the solution on the time step asked. To have the same order of accuracy, the Implicit scheme was discretized with a time step equal to $\Delta \bar{t} = 1 \cdot 10^{-3}$ and a spatial step of $\Delta \bar{x} = 5 \cdot 10^{-3}$. One can observe that the number of modes of the Parametric-SROM approach is higher. Moreover, the discretization of the implicit scheme is very refined. This happened because the Aggregate concrete material has a very slow diffusion process with a low value of the diffusivity coefficient, which concentrates high gradients near the left boundary and slows down the moisture diffusion through the material.

4.2.1 Numerical features

The Parametric-SROM model applies two different techniques of spectral methods, the TAU–GALERKIN approach for the spatial basis function and the Collocation method for the parameter basis function. Both basis functions are the CHEBYSHEV polynomials. The classical collocation points for the CHEBYSHEV basis are the extrema points [27]. However, as the application is not the classical one, different collocation points have been tested as presented in Table 2. As a matter of fact, the best collocation points are the value of the respective parameter to be simulated because during the simulation these actual values of the parameter are required.

Collocation points ν_k	$\varepsilon_{\infty,\nu}$
Itself	$3.79 \cdot 10^{-3}$
Extrema	$1.22 \cdot 10^{-1}$
Equi-spaced	$1.13 \cdot 10^{-1}$

Table 2. Error ε_∞ for the solution of each parameter for different collocation points.

The error ε_2 is shown as a function of space for each material in Figure 8(a) for the Parametric-SROM solution and in Figure 8(b) for the Implicit solution. The methods are built to give a minimum order of accuracy, around $\mathcal{O}\left(10^{-3}\right)$. As the value of the moisture diffusivity coefficient increases, the error decreases because the diffusion process becomes less stiff to solve. It can be noticed that the Implicit scheme faces difficulties to treat the oscillations at the left boundary while the Spectral parametric has a solution more homogeneous over space.
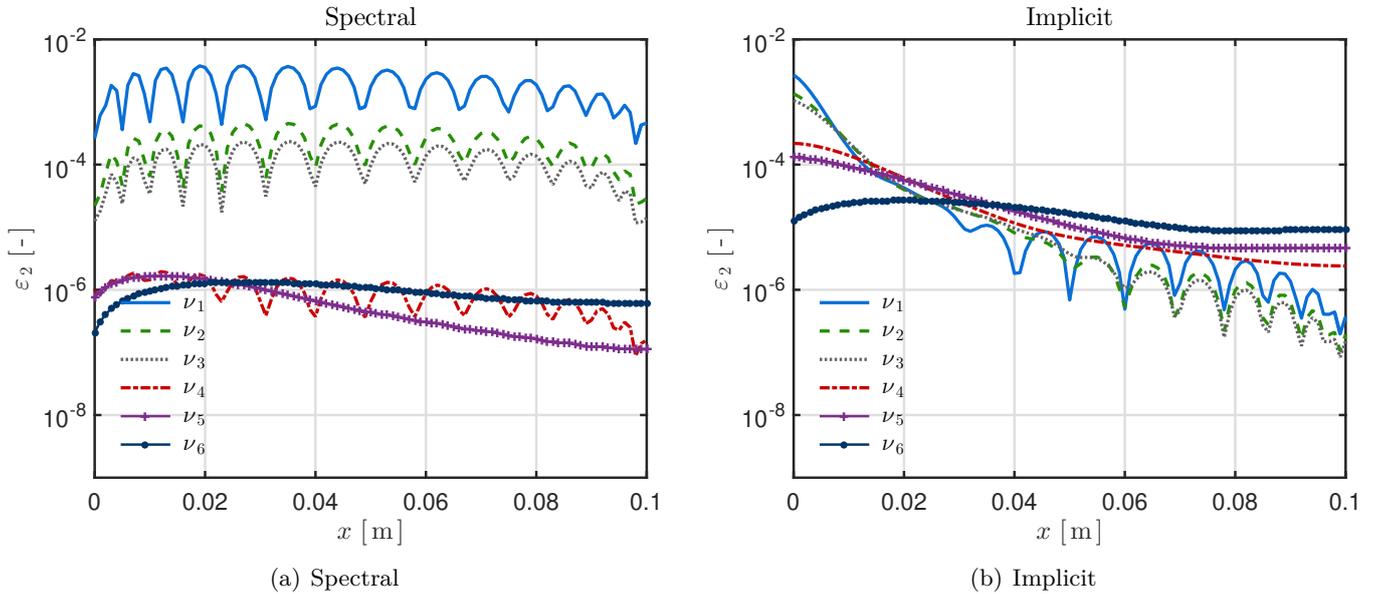

(a) Spectral

(b) Implicit

Figure 8. Error ε_2 computed for the Parametric-SROM solution (a) and also computed for the Implicit solution.

Figure 9(a) presents the last spectral coefficients of the solutions. The magnitude of the spectral coefficients is higher than the error of the solution $\mathcal{O}\left(10^{-6}\right)$ for $\nu_{\max}$ and $\mathcal{O}\left(10^{-3}\right)$ for $\nu_{\min}$. It happens because the collocation points do not correspond for the optimal convergence of the solution. They are chosen according to the specific value of the parameter ν_k. Thus, the *Theorem 6* [17, Page 47] is not valid for this specific case. Nevertheless, if one works with an interval of variation of the parameter (and not determined values), the collocation points can be chosen in their optimal way. In this case, the order of magnitude of the last coefficients would be closer to the order of the error.

Figure 9(b) shows the FOURIER power spectrum function of the signal frequency per unit of time, gener-

ated by the fast FOURIER transform. The peak on the energy is due to the sinusoidal signal at the boundary, since it is the only parameter that interferes on the transient solution.
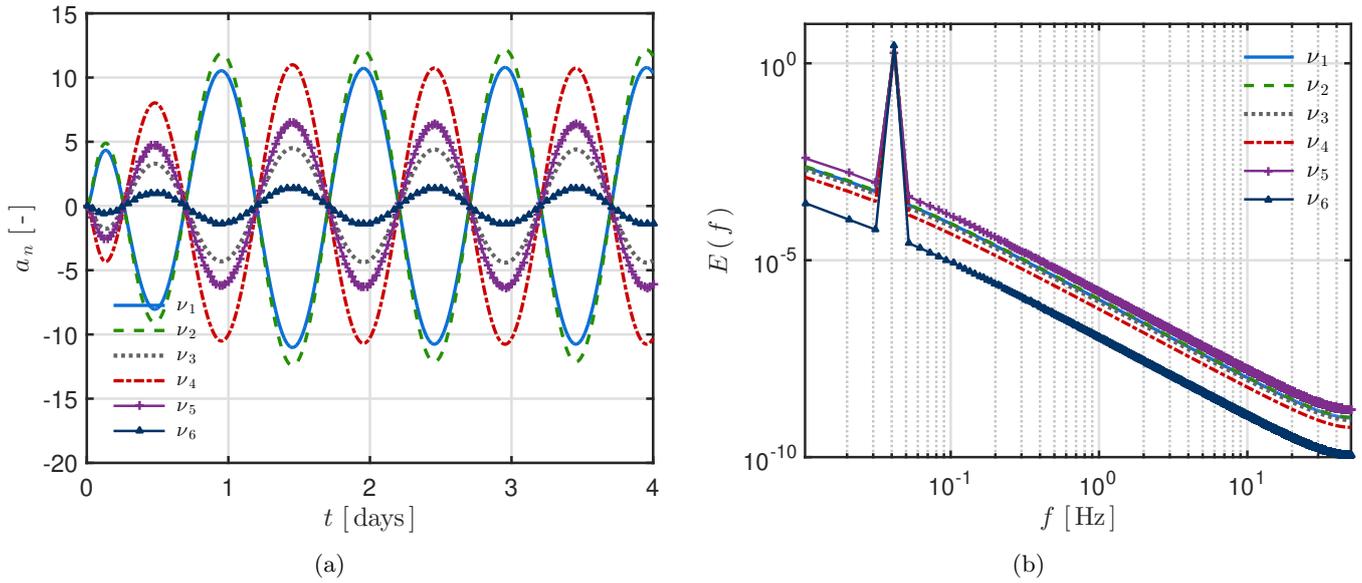

(a)

(b)

Figure 9. Last spectral coefficients (a) and the Fourier Power Spectrum at the left boundary (b) for each material.

The convergence of the basis function of the parameters is presented in Figure 10(a). As it can be observed, it drops at different rates with the increase of the number of modes. Up to 8 parameters the ideal number of modes or collocation points is the quantity of parameters itself. For more than 8 parameters, it does not worth to increase the number of modes because the computational efforts are not saved. The computational run time of each simulation is presented in Figure 10(b). As it can be observed, between $M = 10$ and $M = 15$ modes the computational cost doubles. The computational run time increases because there is still $N = 19$ modes of the spatial basis function. Thus, the number of degrees of freedom for these two cases are $N \cdot M = 19 \cdot 10 = 190$ and $N \cdot M = 19 \cdot 15 = 285$.
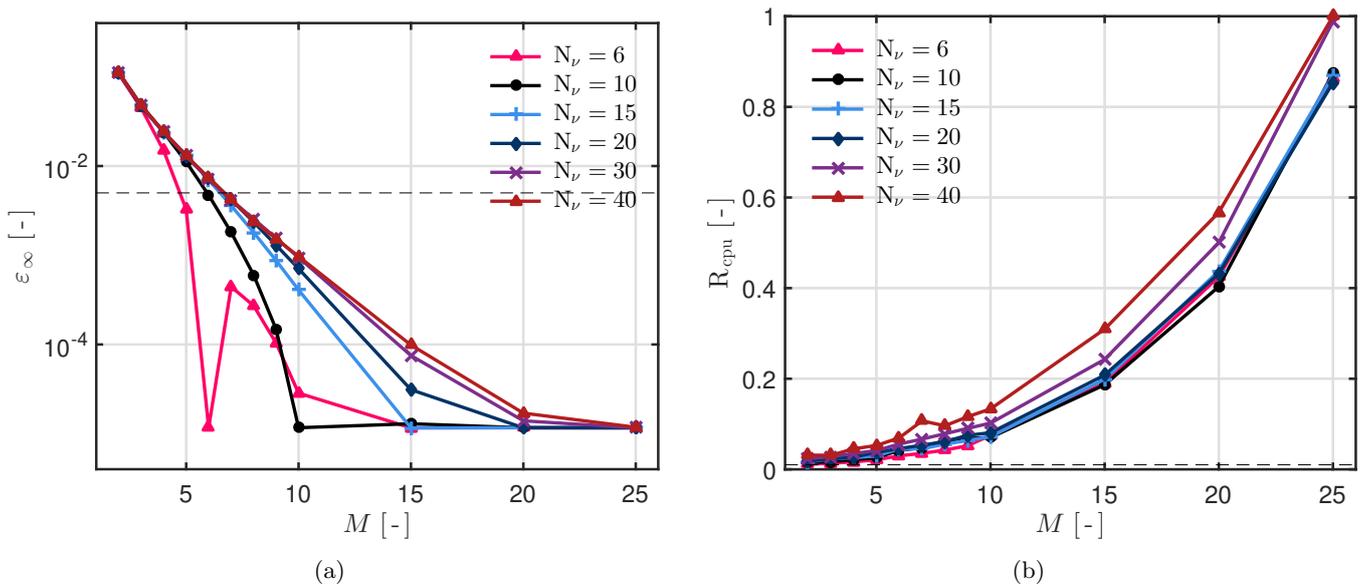

(a)

(b)

Figure 10. Convergence of the Spectral modes M (a) and its computational run time (b) for different quantities of parameters ν_k.

4.2.2 Computational cost

The Parametric-SROM is also compared with the Spectral solution using a loop over the values of the parameter. Both solutions are computed using the same quantity of modes for the spatial basis $N = 19$ and the same tolerance of the solver $\mathsf{tol} = 10^{-5}$. The computational time is presented in Table 3. Both spectral approaches are able to compute the solution of the parametric problem faster than the reference solution and the Implicit scheme, for the same order of accuracy. If the computational time of the implicit method is extrapolated, it will lead to a simulation time of 38 min/year. Looking at four materials and four thicknesses, for example (16 cases), it leads to a computational cost of more than $10h$. It is high value, but not prohibitive. If we add more layers and coupled it to the heat transfer it will grow. Therefore, the use of reduced order models is recommended. In addition, the computational time of the Parametric-SROM is slightly higher than the Spectral solution using a loop. This occurs because the number of modes in the Parametric-SROM approach increases by considering a new parameter as another coordinate, making the integration in time slower than computing the solution for each parameter [18].

Method	$\varepsilon_{\infty,\nu}$	t_{cpu}	R_{cpu}
Reference (loop)	—	132.35 s	5.27
Implicit (loop)	$2.71 \cdot 10^{-3}$	25.10 s	1
Parametric-SROM	$3.79 \cdot 10^{-3}$	5.29 s	0.21
Spectral (loop)	$3.79 \cdot 10^{-3}$	2.06 s	0.08

Table 3. Computational time required to compute the parametric problem and the error $\varepsilon_{\infty,\nu}$ of solution for $\mathrm{N}_\nu = 6$.

Figure 11 shows the computational run time as a function of the number of elements of the parameter ν_k. As expected, the large original model, based on the Implicit scheme requires an important extra time to compute the parametric solution. Both Spectral approaches have significantly reduced the computational cost compared to the large-original model. One interesting result is that the Parametric-SROM model becomes more interesting when the solution has to be computed for more than 30 values of the parameter. The computational time of the Parametric-SROM and the Spectral-loop are almost the same. This occurs because the number of modes M stops growing after 8 parameters, which are enough to give a solution with a minimum order of accuracy around $\mathcal{O}(10^{-3})$. Therefore, if one needs to compute a parametric solution with a large number of these parameters the Parametric-SROM model would be strongly recommended.
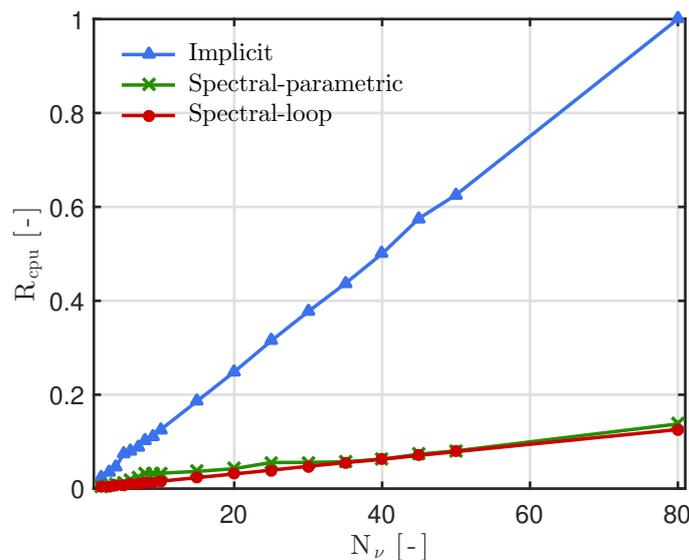

Figure 11. Computational time t_{cpu} as a function of the number of elements N_ν.

The advantage of the Parametric-SROM method is related to its ability to compute *at once* the solution

depending on the three coordinates, whereas the Spectral and the Implicit approaches compute the solution for each value of the desired parameter independently one-by-one with a loop. It should be noted that the Implicit approach is a low-order approximation that provides a solution less accurate than the one obtained by the spectral ones.

5 Parametric problem regarding the material thickness

The case study in this section considers a wall composed of two materials. The parametric analysis is performed regarding the thickness of the material facing the interior of the building.

Here, the parametric problem is solved regarding the time t, the space x and the insulation thickness β_2. Thus, the family of solutions sought are:

$$P_{v,2} \; : \; \mathcal{I}_x \times \mathcal{I}_t \times \mathcal{I}_{\beta_2} \; \longrightarrow \; \mathbb{R} \,, \tag{20}$$

$$(x, \, t, \, \beta_2) \; \longmapsto \; P_v \, (x, \, t, \nu_2) \,, \tag{21}$$

where $\nu \; : \; [\beta_{2,\mathrm{min}}, \, \beta_{2,\mathrm{max}}] \; \longrightarrow \; [\nu_{\mathrm{min}}, \, \nu_{\mathrm{max}}]$ is defined as a coordinate of the problem, with $k_{m,2}$, $c_{m,2}$, L_2 and t_{ref} fixed as constants. So we have a second layer thickness parametric solution. By making the ν vary we are actually working with the variations of β_2 as indicated in Figure 12. Thus, by using the dimensionless formulation the only value that varies is the ν number.
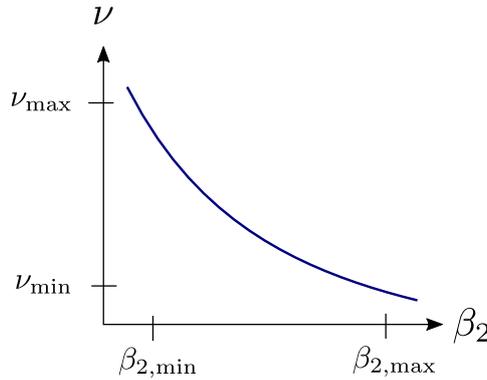

Figure 12. Mapping of the parametric problem regarding the diffusivity.

The problem is solved by means of the parametric spectral-reduced-order model.

5.1 Description of the case study

For this case, we seek for a parametric solution of Equation (3) regarding the thickness of the material facing the interior of the building. The vapor pressure is computed as a function of time t, space x and the thickness L_2 of the second layer as depicted in Figure 13.

The exterior side of the wall is exposed to cyclic changes of relative humidity between $33\,\%$ and $73\,\%$, and the interior side changes between $33\,\%$ and $83\,\%$ with a $24\,\mathsf{h}$ period. The total time of simulation is five days or $120\,\mathsf{h}$. The convective vapor transfer coefficient is equal to $h_m^L = 5 \cdot 10^{-7}\,\mathsf{s/m}$ at the exterior side and $h_m^R = 2 \cdot 10^{-8}\,\mathsf{s/m}$ at the interior side. The initial condition is homogeneous within both materials with a vapor pressure value of $P_{v,\mathrm{i}} = 925.46\,\mathsf{Pa}$. Simulations undergo at a constant $23°\mathsf{C}$ temperature that leads to a saturation pressure of $2804.4\,\mathsf{Pa}$. The first layer is 15-cm thick and the second layer thickness is evaluated in the parametric problem:

$$
\begin{aligned}
L_1 \;&=\; 0.15\;[\mathsf{m}] \,, & \beta_1 &= 1, \\
L_2 \;&=\; 0.10\;[\mathsf{m}] \,, & \beta_2 &\in [1, \, 2] \,.
\end{aligned}
$$

The first layer is composed of cellular concrete and the second layer is composed of an insulation material. The properties of both materials are given in Table 4.
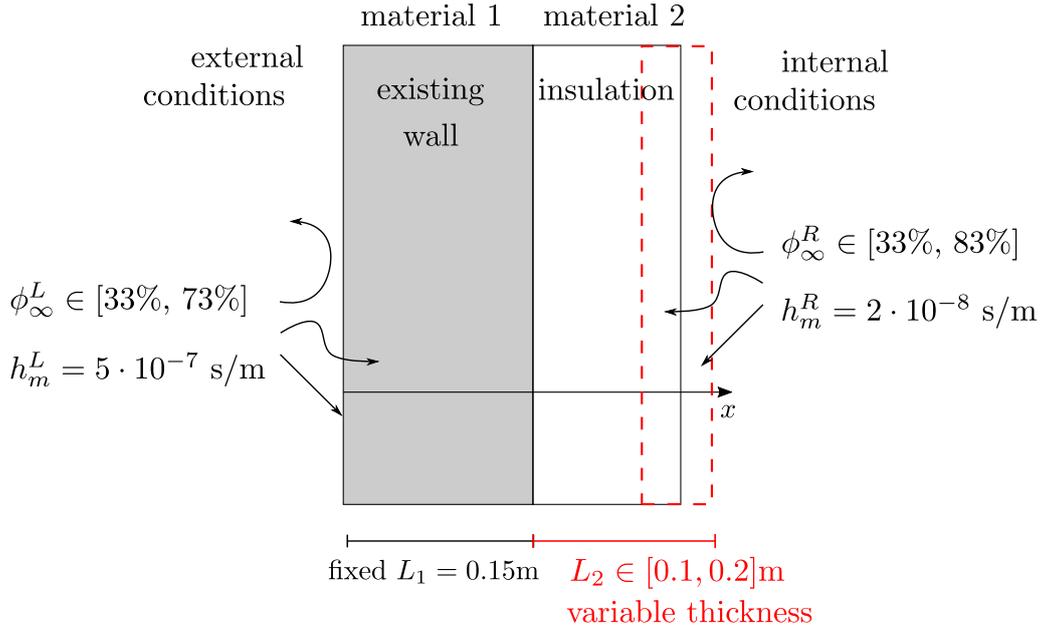
Figure 13. Scheme of the wall to be renovate.

Material	*Storage coefficient* c_m [kg/(m³.Pa)]	*Transfer coefficient* k_m [s]	*Diffusivity* ν [m²/s]
Aggregate concrete	$5.08 \cdot 10^{-2}$	$1 \cdot 10^{-11}$	$1.97 \cdot 10^{-10}$
Insulation	$7.49 \cdot 10^{-3}$	$1.3 \cdot 10^{-9}$	$1.74 \cdot 10^{-7}$

Table 4. Properties of the materials used in the multi-layered case [31].

5.2 Results and discussion

Simulations are performed for different values of the thickness $\{0.1, 0.125, 0.15, 0.175, 0.2\}$ m. The Parametric-SROM model is compared with the reference solution, obtained with the `Chebfun` toolbox.
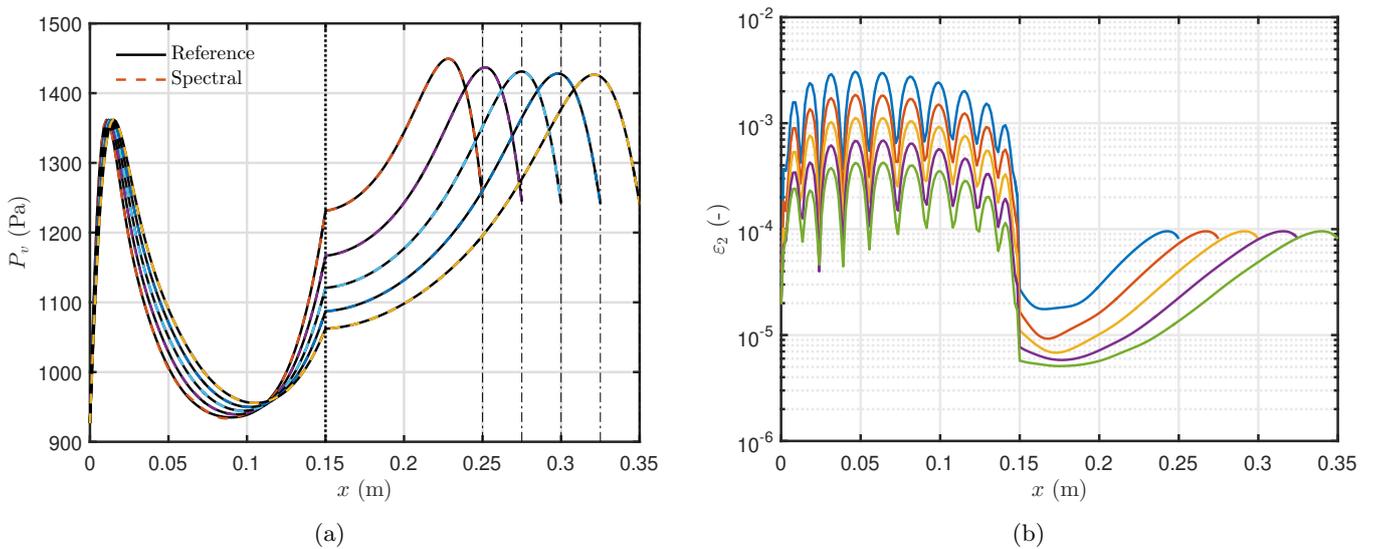

(a)

(b)

Figure 14. Vapor pressure profiles for each thickness value at $t = 48$ h (a), and the respective error ε_2 for each thickness parameter (b).

Figure 14(a) shows the profiles of vapor pressure within each material at the time instant $t = 48\,\mathrm{h}$. It is possible to observe significant variations of the vapor pressure within each material as the thickness increases. The error ε_2 is shown as a function of space for each material in Figure 14(b) for the Parametric-SROM solution. The accuracy is at order of $\mathcal{O}\left(10^{-3}\right)$. The error on the first layer is higher because the material has a low diffusivity, which makes the problem stiffer, and the accuracy decreases. As the thickness of the material increases, the error decreases because the diffusion process becomes less stiff to solve.
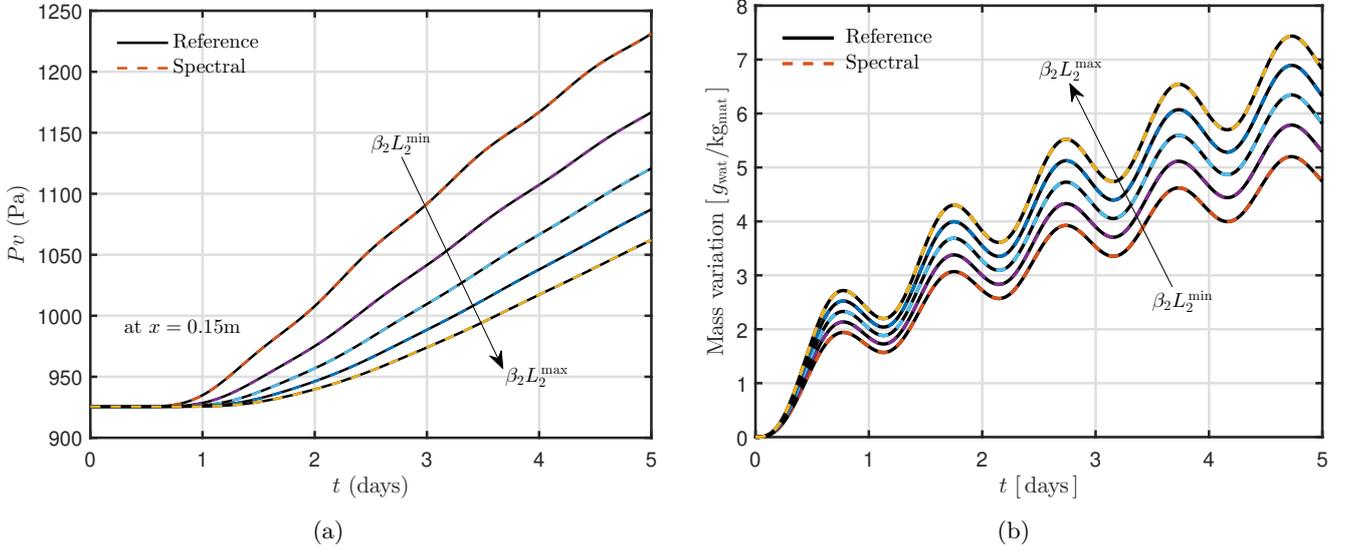

(a)

(b)

Figure 15. Vapor pressure evolution at the interface, (a) and the mass variation over the wall (b).

Furthermore, Figure 15(a) presents the evolution of vapor pressure at the interface between materials. In this figure, the Parametric-SROM approach is in good agreement with the reference solution. The thicker the insulation the lower the vapor pressure at this location, as moisture penetration takes longer. In contrast, Figure 15(b) illustrates the evolution of moisture content for the two materials, showing that the thicker the insulation, the higher the water accumulation.

6   Case study with wind-driven rain

In the present case study, we simulate a wall composed of two materials, aggregate concrete and insulation, which properties are presented in Table 4. The parametric analysis is performed regarding the inner material thickness, similar to the previous case, as shown in Equation (21).

6.1   Description of the case study

The exterior boundary conditions are implemented according to the weather data file for La Rochelle, a French coastal city with a tempered oceanic climate. This climate is known for relatively hot summers and mild winters. The vapor pressure and the source term relative to the driving rain are given in Figures 16(a) and 16(b), for a whole year. The weather data is taken from the Meteonorm database, which is representative of the mean values over the last 30 years (TMY2 format). The signal is filtered using a rational transfer function of Matlab integrate on the function *filter* for one-dimensional input data.

The outdoor ambient vapor pressure is calculated from the relation $P_v = \phi \cdot P_{sat}(T)$. The wind-driven rain is calculated from the Lacy's model, which is based on empirical relations:

$$g_\infty = \frac{2}{9} U_w R_h^{8/9} \tag{22}$$

where $U_w[m/s]$ is the wind speed and $R_h[mm/s]$ is the horizontal rainfall rate. This relation is valid for a building in an open field location. For the indoor boundary conditions, we consider cyclic variations of
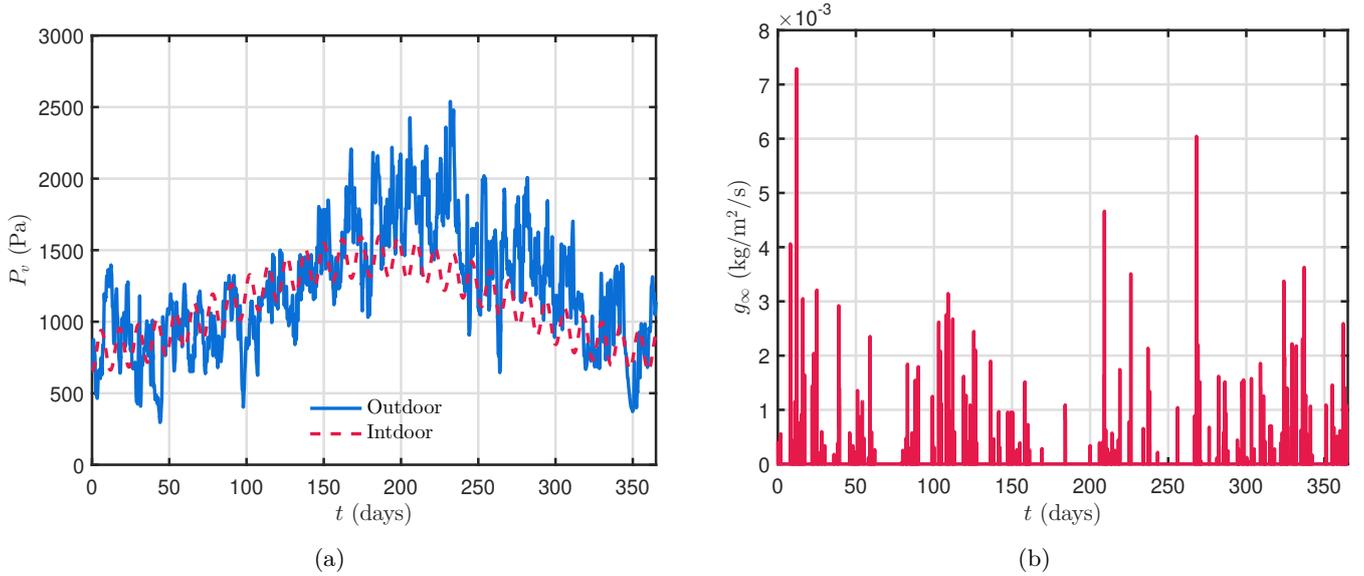
Figure 16. Outdoor and indoor ambient vapor pressure (a) and wind driven rain source term (b).

the vapor pressure between $600\,\mathrm{Pa}$ and $2200\,\mathrm{Pa}$. The total time of simulation is thirty days for verification and then one year simulation for further analysis. The convective vapor transfer coefficient is of $h_m^L = 5 \cdot 10^{-7}\,\mathrm{s/m}$ at the exterior side and $h_m^R = 2 \cdot 10^{-8}\,\mathrm{s/m}$ at the interior side. The initial condition is homogeneous along the thicknesses of both materials, with a vapor pressure value of $P_{v,\mathrm{i}} = 654.9\,\mathrm{Pa}$, which is equivalent to a $97\,\%$ relative humidity and a temperature of $0.7°\mathrm{C}$. The first layer is 10-cm thick and the second layer thickness varies according to Equation (21). The material properties are given in Table 1.

For this case, we seek for a parametric solution of Equation (3) regarding the inner material thickness. The vapor pressure is computed as a function of time t, space x and the thickness L_2 of the second layer as depicted in Figure 13.

6.2   Results and discussion

Simulations are performed for different values of the thickness $\beta_2\,L_2 = \{0.1, 0.125, 0.15, 0.175, 0.2\}\,\mathrm{m}$. The Parametric-SROM model is compared with the reference solution, obtained with the `Chebfun` toolbox for the first 30 days.

Figure 17(a) shows the evolution of vapor pressure at the left boundary and at the interface between materials. It is possible to observe some peaks on the spectral solution with the incoming of the rain which leads to a higher difference regarding the reference solution. The source term on the boundary conditions leads to an increase on the stiffness of the solution, which is hard for the spectral method to deal with. However, the solution stabilizes right after. The error ε_2 is shown as a function of space in Figure 17(b). The accuracy is at order of $\mathcal{O}\left(10^{-2}\right)$, which is acceptable for our simulations. The error on the left boundary is higher because of the rain but at the interface between materials the solution is very precise, at order of $\mathcal{O}\left(10^{-5}\right)$.

Simulations with `Chebfun` are not performed for the whole year due to the computation cost. It is a good option for reference and comparison. However, it has a high computational expense. In this case, for only one month of simulation, it took approximately 20 min of computer run time. The same simulation time was used by the spectral method to simulate the whole year. Thus, Figure 18(a) presents the evolution of vapor pressure at the internal and external boundaries for the simulation of ν_1. We present the vapor pressure evolution because it is the potential used for the simulations. We can observe the influence of the the wind-driven rain on the first material layer. Figure 18(b) presents the FOURIER power spectrum as a function of the signal frequency per unit of time for the first parameter simulation. The signal at the left boundary, whcih is exposed to the outdoors, is noisy due to the meteorological data. The signal is smooth
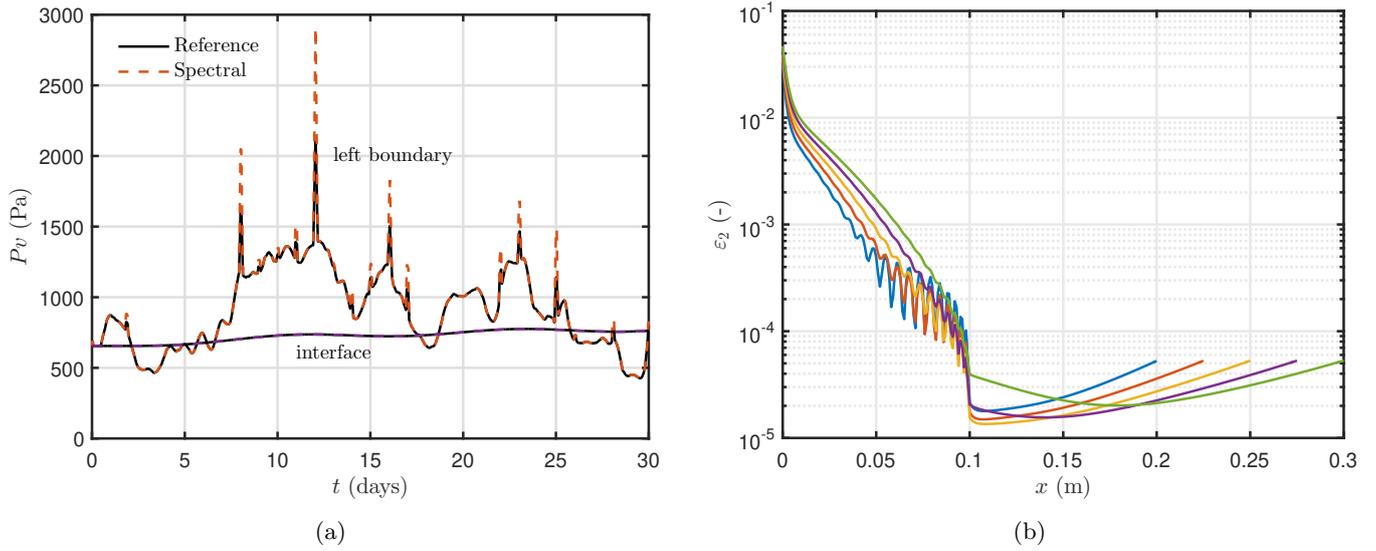
Figure 17. Vapor pressure evolution for the first parameter ν_1 at left boundary and at the interface between materials (a), and the error ε_2 for each thickness parameter (b).
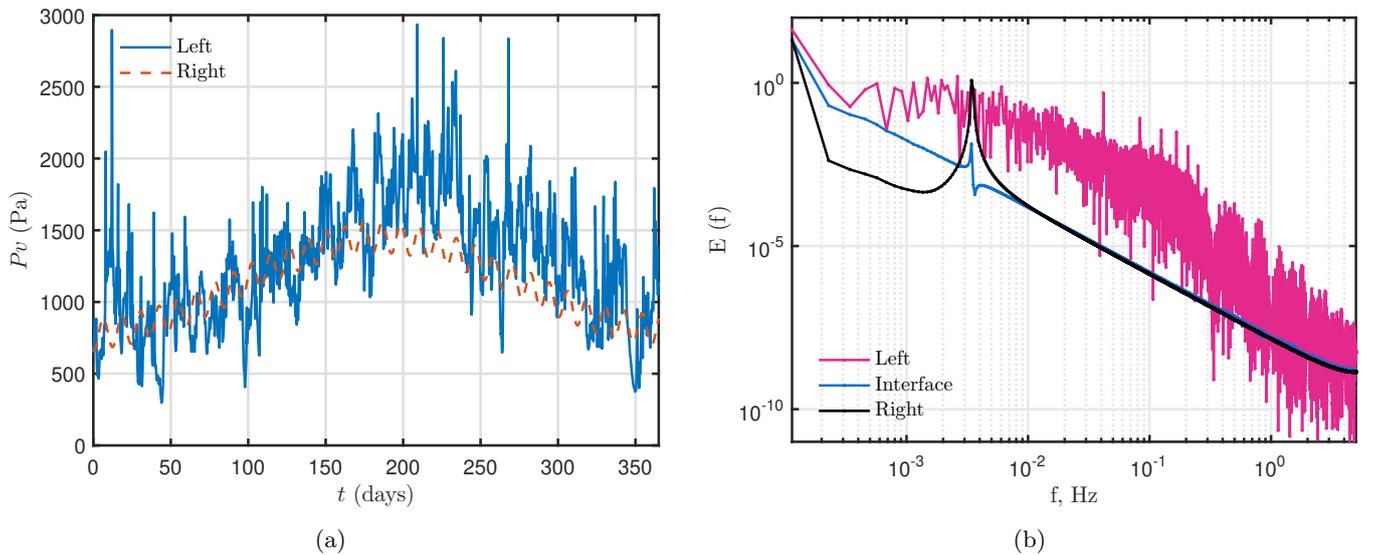

Figure 18. Vapor pressure evolution at the boundaries, (a) and the Fourier power spectrum (b), for the first parameter ν_1.

at the interface, which implies a slow diffusion over the two materials. At the right boundary, the signal has two peaks that are due to the double sinusoidal function imposed.

The relative humidity and the moisture content are common parameters used in the literature to asses the risk of moisture disorders. Therefore, Figures 19(a) and 19(b) present these two indicators. In the Figure 19(a) at the left, we have the relative humidity at $x = 0.01\,\mathrm{m}$ for each one of thickness values. The smaller the thickness the lower the amplitude of variation of the relative humidity as there is less material to adsorb. Figure 19(b) presents the mass variation with time for all the thickness values. The values above the horizontal dashed line represents the risk of appearance of moisture disorders. The references values are of 80% of relative humidity and $20\,g/kg$ of the mass variation, for risk of mold and fungal appearance in commonly used building materials [1, 32]. The dew point is also an interesting way to asses the envelop failure. However, since we have assumed constant temperature, it has not been taken to account. As shown in Figure 19(a), the rain has a local influence, with a 2-cm penetration depth, while the external relative
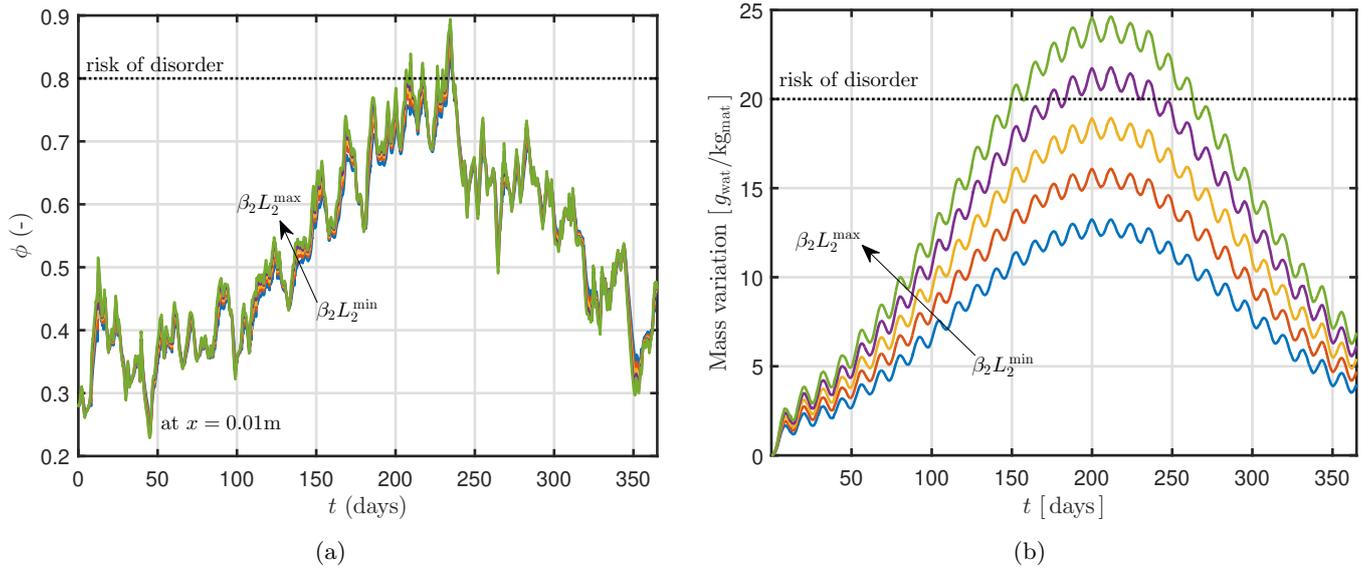
Figure 19. Evolution of the relative humidity within the concrete layer at $x = 0.01\mathrm{m}$, (a) and of the mass variation over the two layers wall (b), for each parametric value.

humidity influences the simulations more globally. The parametric solution allows to analyse the physical phenomena to give the best options. In this case study, the risk of moisture disorder appears for insulations thicker than 0.15 cm as the layer retains more moisture.

The threshold here considered is a simplified example. It is important to note, that the mold growth is also dependent on the temperature and the assumption here is under constant temperature. In addition, depending on the nature of the insulating material, the sorption property should be different and a moisture-friendly insulating material (such as hemp and wood) might still provide acceptable performances for such a mass variation. Therefore, for future works, it is important to consider the coupled heat and moisture transfer to better identify the mold growth risk.

6.3 Extension of the proposed method

In this paper, it was proposed the use the Spectral reduced order model to solve moisture diffusive parametric problems. Indeed, in building applications, more complex phenomena must be addressed, such as the number of layers and varying parameters, the temperature dependency and the whole building simulation. The complexity of implementation will increase but it is a possibility of future work. What was presented in this paper are the first steps.

The Parametric-SROM can be extended to more than one parameter. This is the first step to more complex work considering several extra-parameteres. For additional parameters we can also use orthogonal polynomials. It will be like solving multidimensional problems. The computational cost will increase, approximately proportional to 10^n, with n being the number of dimensions. Depending on how the dimensionlessization is written, more than one parameter at time can be evaluated without adding extra dimension to solve the problem.

The coupled heat and mass transfer is the most important extension of the presented study. Specially with the mold risk and moisture disorders depending on both temperature and relative humidity. In the literature, only heat or mass parametric problems have been addressed. The present work is a first step before solving heat and moisture transfer to parametric problem. The difficulty in solving the coupled parametrized equation is the complexity of the discretization and the inter-dependency on the fields. The size of the discretized matrix on the reduced system will increase and also the computational cost but the formulation will be very similar, with the orthogonal polynomial and the collocation points.

The proposed methodology can be applied to solve parameter problems to the building scale. It can be

performed for different kinds of boundary conditions,such as, Dirichlet, Neumann and Robin. It is possible to couple the diffusion equation with the mass balance at the room scale, which is an important feature for applications at the building scale for energy or comfort assessment. It is feasible but the implementation and development part requires some work. In the building scale, all the equations involved in building physics, such as air energy balance equations, air leakages models must me re-implemented to be solved in terms of the parametric problem. It requires a complex development work that can be seen as perspective of work.

7 Conclusions

This work was devoted to exploring the use of an innovative reduced-order approach based on spectral methods for solving parametric problems. If we write the problem in a dimensionless form, we can solve the problems regarding other parameters aside from space and time.

The first case study considered a linear diffusive moisture transfer through a porous material and the third parameter - aside space and time - was the diffusivity. By using the Spectral reduced-order model the spatial domain is decomposed in three parts and the interface conditions can be easily imposed. As the complexity of the problems rises, the Spectral method needs more modes, with still a very low computational time compared to standard approaches, and yet it does not mean that the spectral method loses its efficiency. Results showed that the spectral approach is faster than the classical implicit approach and we can solve the problem at once. The second case considered a wall composed of two materials and the third parameter analyzed was the insulation thickness. The accuracy of the approach has been demonstrated by representing accurately the physical phenomenon, with an absolute error of the order of $\mathcal{O}\left(10^{-5}, 10^{-2}\right)$ compared to the reference solution, which was obtained.

Moreover, we considered meteorological data and the influence of rain. Simulations are performed for one-year period and by means of the spectral parametric solution, the best thickness values for the selected weather could be determined. Unlike traditional methods such as finite differences/volumes, the application of spectral methods is not straightforward, neither intuitive. Although, the efforts used in its implementation are compensated by the results, which showed to be very promising. One interesting outlook is to use the Parametric-SROM solution for non-linear heat and moisture transfer and the extension to the whole building simulation.

Acknowledgement

Disclosure statement

No potential conflict of interest was reported by the authors.

Nomenclature

Latin letters

c_w	liquid water specific heat	$[\mathsf{J}/(\mathsf{kg}\cdot\mathsf{K})]$
c_m	moisture storage coefficient	$[\mathsf{s}^2/\mathsf{m}^2]$
h_m	convective vapor transfer coefficient	$[\mathsf{s}/\mathsf{m}]$
g_∞	liquid flow	$[\mathsf{kg}/(\mathsf{m}^2\cdot\mathsf{s})]$

g	flow	$[\text{kg}/(\text{m}^2 \cdot \text{s})]$
k_l	liquid permeability	$[\text{s}]$
k_m	moisture transf. coeff. under vap. press. grad.	$[\text{s}]$
L	thickness	$[\text{m}]$
$\mathbf{n}$	normal space, that assumes either $+1$ or -1	$[-]$
P_s	saturation pressure	$[\text{Pa}]$
P_v	vapor pressure	$[\text{Pa}]$
q	heat flux	$[\text{W/m}^2]$
R_v	water gas constant	$[\text{J}/(\text{kg} \cdot \text{K})]$
R_h	horizontal rainfall rate	$[\text{mm/s}]$
T	temperature	$[\text{K}]$
U_w	wind speed	$[\text{m/s}]$
w	moisture content	$[\text{kg/m}^3]$

Greek letters

ν	moisture diffusivity	$[\text{m}^2/\text{s}]$
δ_v	vapor permeability	$[\text{s}]$
ϕ	relative humidity	$[-]$
ρ	specific mass	$[\text{kg/m}^3]$

Dimensionless parameters

Bi	Biot number	$[-]$
ν	Fourier number	$[-]$
u	vapor pressure	$[-]$

Abbreviation

MBV	Moisture Buffer Value
ODE	Ordinary Differential Equation
PGD	Proper Generalized Decomposition
ROM	Reduced Order Model
SROM	Spectral Reduced Order Model

References

[1] J. Berger, S. Guernouti, M. Woloszyn, and C. Buhe, "Factors governing the development of moisture disorders for integration into building performance simulation," *Journal of Building Engineering*, vol. 3, pp. 1–15, 2015. 1, 21

[2] J. Huang, S. Wang, F. Teng, and W. Feng, "Thermal performance optimization of envelope in the energy-saving renovation of existing residential buildings," *Energy and Buildings*, vol. 247, p. 111103, 2021. 1

[3] N. Aste, A. Angelotti, and M. Buzzetti, "The influence of the external walls thermal inertia on the energy performance of well insulated buildings," *Energy and Buildings*, vol. 41, no. 11, pp. 1181–1187, 2009. 1

[4] M. Labat, C. Magniont, N. Oudhof, and J.-E. Aubert, "From the experimental characterization of the hygrothermal properties of straw-clay mixtures to the numerical assessment of their buffering potential," *Building and Environment*, vol. 97, pp. 69–81, 2016. 1

[5] M. Ibrahim, P. H. Biwole, P. Achard, E. Wurtz, and G. Ansart, "Building envelope with a new aerogel-based insulating rendering: Experimental and numerical study, cost analysis, and thickness optimization," *Applied Energy*, vol. 159, pp. 490–501, 2015. 1

[6] S. Al-Sanea and M. Zedan, "Improving thermal performance of building walls by optimizing insulation layer distribution and thickness for same thermal mass," *Applied Energy*, vol. 88, no. 9, pp. 3113–3124, 2011. 2

[7] D. Bond, W. Clark, and M. Kimber, "Configuring wall layers for improved insulation performance," *Applied Energy*, vol. 112, pp. 235–245, 2013. 2

[8] S. Gasparin, J. Berger, D. Dutykh, and N. Mendes, "An innovative method to determine optimum insulation thickness based on non-uniform adaptive moving grid," *Journal of the Brazilian Society of Mechanical Sciences and Engineering*, vol. 41, no. 173, pp. 1–18, 2019. 2

[9] E. Pruliere, F. Chinesta, and A. Ammar, "On the deterministic solution of multidimensional parametric models using the proper generalized decomposition," *Mathematics and Computers in Simulation*, vol. 81, no. 4, pp. 791–810, 2010. 2

[10] J. Berger, N. Mendes, S. Guernouti, M. Woloszyn, and F. Chinesta, "Review of reduced order models for heat and moisture transfer in building physics with emphasis in PGD approaches," *Archives of Computational Methods in Engineering*, vol. 24, pp. 655 –667, 2017. 2

[11] J. Berger and N. Mendes, "An innovative method for the design of high energy performance building envelopes," *Applied Energy*, vol. 190, pp. 266–277, 2017. 2

[12] M.-H. Azam, S. Guernouti, M. Musy, J. Berger, P. Poullain, and A. Rodler, "A mixed POD–PGD approach to parametric thermal impervious soil modeling: Application to canyon streets," *Sustainable Cities and Society*, vol. 42, pp. 444–461, 2018. 2

[13] M.-H. Azam, J. Berger, S. Guernouti, P. Poullain, and M. Musy, "Parametric PGD model used with orthogonal polynomials to assess efficiently the building's envelope thermal performance," *Journal of Building Performance Simulation*, vol. 14, no. 2, pp. 132–154, 2021. 2

[14] S. Gasparin, D. Dutykh, and N. Mendes, "A spectral method for solving heat and moisture transfer through consolidated porous media," *International Journal for Numerical Methods in Engineering*, vol. 117, no. 11, pp. 1143–1170, 2019. 2

[15] S. Oh, "An efficient spectral method to solve multi-dimensional linear partial different equations using chebyshev polynomials," *Mathematics*, vol. 7, no. 1, 2019. 2

[16] L. Trefethen, *Finite Difference and Spectral Methods for Ordinary and Partial Differential Equations*. Ithaca, NY, USA: The author, 1996. 2

[17] J. P. Boyd, *Chebyshev and Fourier Spectral Methods*. New York: Dover Publications, second edition ed., 2000. 2, 8, 14

[18] S. Gasparin, J. Berger, D. Dutykh, and N. Mendes, "Advanced reduced-order models for moisture diffusion in porous media," *Transport in Porous Media*, vol. 124, pp. 965–994, Sep 2018. 2, 16

[19] J. Berger, M. Chhay, S. Guernouti, and M. Woloszyn, "Proper generalized decomposition for solving coupled heat and moisture transfer," *Journal of Building Performance Simulation*, vol. 8, no. 5, pp. 295–311, 2014. 2

[20] S. Gasparin, J. Berger, D. Dutykh, and N. Mendes, "Solving nonlinear diffusive problems in buildings by means of a spectral reduced-order model," *Journal of Building Performance Simulation*, vol. 12, no. 1, pp. 17–36, 2019. 2, 7, 9

[21] M. Funk and K. G. Wakili, "Driving potentials of heat and mass transport in porous building materials: A comparison between general linear, thermodynamic and micromechanical derivation schemes," *Transport in Porous Media*, vol. 72, pp. 273–294, 2008. 3

[22] S. Rouchier, M. Woloszyn, G. Foray, and J. Roux, "Influence of concrete fracture on the rain infiltration and thermal performance of building facades," *International Journal of Heat and Mass Transfer*, vol. 61, pp. 340–352, 2013. 3

[23] V. P. De Freitas, V. Abrantes, and P. Crausse, "Moisture migration in building walls - Analysis of the interface phenomena," *Building and Environment*, vol. 31, no. 2, pp. 99–108, 1996. 4

[24] W. Kahan and J. Palmer, "On a proposed floating-point standard," *ACM SIGNUM Newsletter*, vol. 14, pp. 13–21, 1979. 4

[25] T. A. Driscoll, N. Hale, and L. N. Trefethen, "Chebfun guide," *Pafnuty Publications*, Oxford 2014. 6

[26] J. Taylor, *An Introduction to Error Analysis: The Study of Uncertainties in Physical Measurements*. ASMSU/Spartans.4.Spartans Textbook, University Science Books, 1997. 6

[27] B. Fornberg, *A pratical guide to pseudospectral methods*. New York, USA: Cambridge University Press, 1996. 7, 8, 14

[28] C. Canuto, M. Y. Hussaini, A. Quarteroni, and T. A. Zang, *Spectral Methods - Fundamentals in Single Domains*. Scientific Computation, Berlin, Heidelberg: Springer Berlin Heidelberg, 2006. 8

[29] T. Kolda and B. Bader, "Tensor decompositions and applications," *SIAM Review*, vol. 51, no. 3, pp. 455–500, 2009. 9

[30] C. Rode and R. H. Peuhkur, *The Concept of Moisture Buffer Value of Building Materials and its Application in Building Design*, vol. III, pp. 57–62. 2006. 11

[31] C. Rode, R. Peuhkuri, L. H. Mortensen, K. K. Hansen, B. Time, A. Gustavsen, T. Ojanen, J. Ahonen, J. Ahonen, K. Svennberg, L.-E. Harderup, and J. Arfvidsson, "Moisture Buffering of Building Materials," Tech. Rep. R-126, Department of Civil Engineering Technical University of Denmark, 2005. 12, 18

[32] S. Dedesko and J. A. Siegel, "Moisture parameters and fungal communities associated with gypsum drywall in buildings," *Microbiome*, vol. 3, no. 71, pp. 1–15, 2015. 21

A   Rescaling

To apply the orthogonal polynomials used in this work, some domains must be changed to fit the segment $[-1, 1]$.

A.1 Change of variables on the spatial domain

For this reason, a change in the spatial domain segment $x : [0, \ell] \longmapsto \bar{x} : [-1, 1]$ is carried out on the following system:

$$
\begin{cases}
\dfrac{\partial u}{\partial t} = \nu \cdot \dfrac{\partial^2 u}{\partial x^2}, & x \in (0, 1) \text{ and } t > 0, \\[2mm]
u = f(x), & x \in (0, 1) \text{ and } t = 0, \\[2mm]
\dfrac{\partial u}{\partial x} = \mathrm{Bi}_m^L \cdot \left(u - u_\infty^L \right), & x = 0 \text{ and } t \geqslant 0, \\[2mm]
\dfrac{\partial u}{\partial x} = \mathrm{Bi}_m^R \cdot \left(u - u_\infty^R \right), & x = 1 \text{ and } t \geqslant 0.
\end{cases}
\tag{23}
$$

First, we consider a linear relation between x and $\bar{x}$ such that:

$$
x : \bar{x} \longmapsto a \cdot \bar{x} + b,
$$

where a and b are real constants. To determine their values, we relate the extrema points:

$$
\begin{cases}
x(-1) = 0, \\
x(+1) = 1,
\end{cases}
$$

which leads to:

$$
a = b = \frac{1}{2}.
$$

Then, the function x is written as:

$$
x : \bar{x} \longmapsto \frac{1}{2} \cdot (\bar{x} + 1).
\tag{24}
$$

Substituting Equation (24) in the system of Equation (23) leads to the system:

$$
\begin{cases}
\dfrac{\partial u}{\partial t} = 4 \cdot \nu \cdot \dfrac{\partial^2 u}{\partial \bar{x}^2}, & \bar{x} \in (-1, 1) \text{ and } t > 0, \\[2mm]
u = \bar{f}(\bar{x}), & \bar{x} \in (-1, 1) \text{ and } t = 0, \\[2mm]
\dfrac{\partial u}{\partial \bar{x}} = \dfrac{\mathrm{Bi}_m^L}{2} \cdot \left(u - u_\infty^L \right), & \bar{x} = -1 \text{ and } t \geqslant 0, \\[2mm]
\dfrac{\partial u}{\partial \bar{x}} = \dfrac{\mathrm{Bi}_m^R}{2} \cdot \left(u - u_\infty^R \right), & \bar{x} = 1 \text{ and } t \geqslant 0.
\end{cases}
\tag{25}
$$

A.2 Change of variables on the parametric domain

Similarly, a change in the parametric interval $[\nu_{\min}, \nu_{\max}] \xrightarrow{\bar{\nu}} [-1, 1]$ is carried out for the new system on Equation (25).

Consider a linear relation between ν and $\bar{\nu}$ such that:

$$
\bar{\nu} : \nu \longmapsto a \cdot \nu + b,
$$
$$
\nu : \bar{\nu} \longmapsto \frac{\bar{\nu} - b}{a},
$$

where a and b are real constants. To determine their values, we relate the extrema points:

$$
\begin{cases}
\bar{\nu}(\nu_{\min}) = -1, \\
\bar{\nu}(\nu_{\max}) = 1,
\end{cases}
$$

which leads to:

$$a \;=\; \frac{2}{\nu_{\max} \;-\; \nu_{\min}} \qquad \text{and} \qquad b \;=\; -\,1 \;-\; \frac{2 \cdot \nu_{\min}}{\nu_{\max} \;-\; \nu_{\min}}\,.$$

Then, the function $\bar{\nu}$ is written as:

$$\bar{\nu} \;=\; \frac{2 \cdot (\nu \;-\; \nu_{\min})}{\nu_{\max} \;-\; \nu_{\min}} \;-\; 1\,, \tag{26}$$

and, the function ν is written as:

$$\nu \;=\; \frac{(\nu_{\max} \;-\; \nu_{\min}) \cdot (\bar{\nu} \;+\; 1)}{2} \;+\; \nu_{\min}\,. \tag{27}$$

Substituting Equation (27) in the system of Equation (25) leads to the problem:

$$\begin{cases} \dfrac{\partial u}{\partial t} \;=\; 4 \cdot \left(\dfrac{(\nu_{\max} - \nu_{\min}) \cdot (\bar{\nu} + 1)}{2} + \nu_{\min} \right) \cdot \dfrac{\partial^2 u}{\partial \bar{x}^2}\,, & \bar{x}, \bar{\nu} \;\in\; (-1,\,1) \text{ and } t \;>\; 0\,, \\[2ex] u \;=\; \bar{f}\,(\bar{x})\,, & \bar{x} \;\in\; (-1,\,1) \text{ and } t \;=\; 0\,, \\[2ex] \dfrac{\partial u}{\partial \bar{x}} \;=\; \dfrac{\mathrm{Bi}_m^L}{2} \cdot \left(u \;-\; u_\infty^L \right)\,, & \bar{x} \;=\; -1 \text{ and } t \;\geqslant\; 0\,, \\[2ex] \dfrac{\partial u}{\partial \bar{x}} \;=\; \dfrac{\mathrm{Bi}_m^R}{2} \cdot \left(u \;-\; u_\infty^R \right)\,, & \bar{x} \;=\; 1 \text{ and } t \;\geqslant\; 0\,. \end{cases}$$